AD-A234 391

Technical Document 2034
January 1991

Sea Echo Calculations for HH and VV Polarization

R. A. Pappert

Approved for public release; distribution is unlimited.

91 4 25 012

NAVAL OCEAN SYSTEMS CENTER
San Diego, California 92152-5000

J. D. FONTANA, CAPT, USN
Commander

H. R. TALKINGTON, Acting
Technical Director

ADMINISTRATIVE INFORMATION

Released by
J. A Ferguson, Head
Ionospheric Branch

Under authority of
J. H. Richter, Head
Ocean and Atmospheric
Sciences Division

FS

CONTENTS

CONTENTS (continued)

1.0 INTRODUCTION

Composite model formalism has recently been used for HH polarization studies of clutter in evaporation ducts via waveguide and ray methods[1, 2&*]. Surface normal tilting in the plane of incidence, defined by the incident wave and the unperturbed surface normal, was allowed for in those studies. In this study, both HH and VV polarization is considered with allowance for surface normal tilting both in the plane of incidence and normal to the plane of incidence. Effects associated with surface normal tilting perpendicular to the plane of incidence have been discussed by Valenzuela[3&4] and his formulas, with minor modifications, are used in this study. Though the theory is more generally applicable, the numerical results presented like those of the earlier studies, are restricted to x band.

The significance of surface normal tilting normal to the plane of incidence is that an incident horizontally or vertically polarized wave will, relative to the tilted surface, exhibit both horizontal and vertical components. First order Bragg backscatter theory shows, for complex permittivities typical of the ocean and for grazing incidence angles, that the normalized cross section for vertical polarization significantly exceeds that for horizontal polarization. Thus, polarization mixing due to surface normal tilting normal to the unperturbed plane of incidence can be of significance in determining the HH and VV normalized cross sections.

Allowance for surface tilting normal to the plane of incidence requires averaging over the angles of tilt. Two models are considered in this study. The first model assumes a Gaussian distribution with root mean square (rms) slopes determined from the Pierson spectrum[5]. The second model assumes tilt angles of 30° associated with wedges formed as the waves begin to break. The latter model, as a contributor to the clutter, has been suggested by Kalmykov and Pustovoytenko[6] and by Wetzel[7]. Not surprisingly, in view of previous estimates made by Wetzel[7], even in the most favorable circumstance it is found that at x band the normalized cross section for vertical polarization is about 10 dB higher than the normalized cross section for HH polarization. This is contrary to experiment and suggests that other scattering mechanisms, such as scattering by water spray and droplets, may be playing an active role at x band. Even though other scattering mechanisms may be important it should be possible to couple scattering associated with such mechanisms and the propagators developed in the earlier studies to estimate the backscatter. Even though the normalized cross sections for the cross polarized components HV (VH) could be obtained using this present formalism, no effort has been made to do that in this study.

Model and mathematical preliminaries are given in section 2.0. Discussed in some detail are the quantities to be averaged and how they fit into the path loss formulas previously derived. Section 3.0 contains results for the standard atmosphere and for evaporation ducts[8] with duct heights of 14 and 28 m. The results are for 9.6 GHz and apply to wind speeds of 10, 20, 30, and 40 knots. A general discussion concludes the paper in section 4.0.

---

* Pappert, R.A., R.A. Paulus and F.D. Tappert, "Sea echo in tropospheric ducting environments," submitted to Radio Science. For further information, please contact author.

1

2.0 PRELIMINARIES

Ulaby et al.[9] have treated in detail the problem of first order Bragg backscatter from the sea for horizontal transmit, horizontal receive, HH, and polarization. Their method can be repeated for vertical transmit, vertical receive, VV, and backscatter. This method leads to the conclusion, as asserted by Ulaby et al.[9], that the results for HH polarization can be taken over for VV polarization by simply replacing the sea water permeability, μ (taken to be one), by the sea water permittivity, ϵ, and vice versa. To accommodate this result within the earlier development[1] using waveguide formalism, the path loss formula for both polarizations will be approximated as

$$PL(dB) = -20 Log_{10}\left[1.607 \times 10^3 f_{gh}^2\left(\phi_0 \frac{w_p(2k)}{2k} \frac{\Delta x}{x} G(\theta_{r0}^i) <K_{ii}>\right)^{\frac{1}{2}}\right.$$

$$\left. \cdot \left|\sum_{m,n} \lambda_m^i \lambda_n^i \exp(-jk(\cos\theta_n^i + \cos\theta_m^i)x)e_m^i(z_T)e_n^i(z_T)\right|\right], \tag{1}$$

where

k = rf wave number (m^{-1}),

w_p = Pierson sea spectrum (m^3),

f_{gh} = frequency in gigahertz,

ϕ_0 = one half 3-dB beam width (rad.),

Δx = $c\tau/2$ = spatial pulse length (m)

c = vacuum speed of light (m/s)

τ = pulse length (s),

x = range (m),

G = shadow function,

θ_{r0}^i = real part of grazing eigenangle for least attenuated mode (rad.)

i = polarization index (horizontal polarization, i = h, vertical polarization, i = v)

m, n = mode indices

τ = grazing eigenangle (rad.)

λ = excitation factor,

j = $(-1)^{\frac{1}{2}}$,

e = height gain,

z_T = transmitter and receiver altitude for backscatter configuration (m).

In terms of the angles shown in figure 1 and following the development given on page 970 of Ulaby et al.[9], the quantities, K_{ii}, may be expressed as follows:

2

$$K_{hh} \simeq \sin^4\psi_h \left| \frac{\cos^2(\theta_0^h - a)\Gamma_{hh}}{\cos^2\psi_h(1 + \cos^2 a\tan^2\beta)} + \frac{\sin^2\beta\Gamma_{vh}}{\cos^2\psi_h(1 + \cos^2\beta\tan^2 a)^2} \right|^2 , \tag{2}$$

or

$$K_{hh} \simeq \sin^4\psi_h \left| \frac{(\cos\theta_0^h + \sin\theta_0^h\tan\gamma\cos\phi)^2\Gamma_{hh}}{\tan^2\gamma\sin^2\phi + (\cos\theta_0^h + \sin\theta_0^h\tan\gamma\cos\phi)^2} \right. \tag{3}$$

$$\left. + \frac{\tan^2\gamma\sin^2\phi^2\Gamma_{vh}}{\tan^2\gamma\sin^2\phi + (\cos\theta_0^h + \sin\theta_0^h\tan\gamma\cos\phi)^2} \right|^2$$

$$K_{vv} \simeq \sin^4\psi_v \left| \frac{\cos^2(\theta_0^v - a)\Gamma_{vv}}{\cos^2\psi_v(1 + \cos^2 a\tan^2\beta)} + \frac{\sin^2\beta\Gamma_{hv}}{\cos^2\psi_v(1 + \cos^2\beta\tan^2 a)} \right|^2 , \tag{4}$$

$$K_{vv} \simeq \sin^4\psi_v \left| \frac{(\cos\theta_0^v + \sin\theta_0^v\tan\gamma\cos\phi)^2\Gamma_{vv}}{\tan^2\gamma\sin^2\phi + (\cos\theta_0^v + \sin\phi_0^v\tan\gamma\cos\phi)^2} \right. \tag{5}$$

$$\left. + \frac{\tan^2\gamma\sin^2\phi^2\Gamma_{hv}}{\tan^2\gamma\sin^2\phi + (\cos\theta_0^v + \sin\theta_0^v\tan\gamma\cos\phi)^2} \right|^2 ,$$

where

$$\psi_{v,h} = \cos^{-1}\left[\frac{(\cos^2 a\tan^2\beta + \cos^2(\theta_0^{v,h} - a))^{\frac{1}{2}}}{(1 + \cos^2 a\tan^2\beta)^{\frac{1}{2}}} \right] , \tag{6}$$

or

$$\psi_{v,h} = \cos^{-1}\left(\cos\gamma(\tan^2\gamma\sin^2\phi + (\cos\theta_0^{v,h} + \sin\theta_0^{v,h}\tan\gamma\cos\theta)^2)^{\frac{1}{2}} \right) , \tag{7}$$

$$\Gamma_{hh} = \frac{(\epsilon - 1)}{\left(\sin\psi_h + (\epsilon - \cos^2\psi_h)^{\frac{1}{2}} \right)^2} , \tag{8}$$

$$\Gamma_{vv} = \frac{(\epsilon - 1)\,[\epsilon(1 + \cos^2 \psi_v) - \cos^2 \psi_v]}{\left(\epsilon \sin \psi_v + (\epsilon - \cos^2 \psi_v)^{\frac{1}{2}}\right)^2}, \tag{9}$$

$$\Gamma_{vh} = \frac{(\epsilon - 1)\,[\epsilon(1 + \cos^2 \psi_h) - \cos^2 \psi_h]}{\left(\epsilon \sin \psi_h + (\epsilon - \cos^2 \psi_h)^{\frac{1}{2}}\right)^2}, \tag{10}$$

$$\Gamma_{hh} = \frac{(\epsilon - 1)}{\left(\sin \psi_v + (\epsilon - \cos^2 \psi_v)^{\frac{1}{2}}\right)^2}. \tag{11}$$

The brackets, $< >$, in equation 1 signify averages, subsequently defined to be taken over either pair (α, β) or pair (γ, ϕ). Each pair defines the orientation of the local perturbed surface normal. From figure 1, α will be seen to be the tilt angle in the unperturbed plane of incidence and β the tilt angle in the plane perpendicular to the unperturbed plane of incidence. Similarly, γ is the angle between the local perturbed surface normal, the z axis, and ϕ its azimuth. The quantity $\theta_0^{v,h}$, which appears in the above equations, is the eigenangle for the least attenuated mode. This form of the equations presumes that the rms slope of the perturbed surface is large compared with the magnitudes of the modal eigenangles which contribute significantly to the mode sums. This is justified for the cases reported in this study. In fact with little error (probably on the order of 1 dB) $\theta_0^{v,h}$ can be set to zero, as has been done in generating the results in the following section. The quantities $\psi_{v,h}$ defined by equations (6) and (7) are the local angle of incidence. This is particularly simple to see when $\beta = 0$. Then from equation (6), $\psi_{v,h} = \theta_0^{v,h} - \alpha$ (α is negative for illuminated facets when the incident wave propagates in the positive x and negative z direction). Also from equation (7) with $\phi = \pi$ it follows that $\psi_{v,h} = \theta_0^{v,h} + \gamma$. Valenzuela[4] has given results similar to equations (2) and (4). The current formulas differ from his in terms of $0(\alpha^4, \beta^4, \alpha^2\beta^2)$. It is believed that the coefficients given above are in fact correct to all orders. There is, of course, the significant point that higher order corrections to the coefficients are questionable since the first order Bragg scatter theory upon which equation (1) is founded requires small slopes. Nevertheless, license has been taken and the results in the following section are predicated upon the above equations.

The ray analogue of equation (1) is [2]

$$PL\ (dB) = -10 Log_{10}$$

$$\left(1.486 \times 10^2 f_{gh}^2 \phi_0 \frac{w_p(2k)}{2k} G(\theta_0) < K_{ii} > \frac{\Delta x}{x(n^2(Z_T) - C_0^2)|g''(\theta_0)|^2}\right), \tag{12}$$

where the new quantities appearing in equation (12) are,

$$g''(\theta) = \frac{1}{\sin\theta}\,\frac{d^2}{d\theta^2}\left[x\cos\theta + \left|\int_{z_T}^{0}\left(n^2(z) - \cos^2\theta\right)^{\frac{1}{2}}dz\right|\right]\,,\tag{13}$$

where

ϕ_0 = stationary phase grazing angle,

$n(z)$ = refractive index at height z with $n(o) = 1$,

C_0 = $\cos(\theta_0)$.

The K_{ii} are given by equations (2) through (5) and the Γ's by equations (8) through (11) with the understanding that

$$\theta_o^h = \theta_0^v = \theta_0\,,\ \psi_v = \psi_h,\ \Gamma_{hh} = \Gamma_{hv}\,,\qquad \Gamma_{vv} = \Gamma_{vh}\,.\tag{14}$$

In section 3.0, results associated with two types of averaging will be presented. In the first model (called the "Gaussian model") the slope distribution is taken to be

$$f(a,\beta) = \frac{1}{2\pi s^2}\exp\left(\frac{-(\tan^2 a + \tan^2\beta)}{(2s^2)}\right)\,,\tag{15}$$

where

σ^2 = mean square slope (assumed the same in both the unperturbed incident plane and in the plane normal to it).

Values for the mean square slope as a function of wind speed have been calculated using the Pierson spectrum and have been listed in an earlier work[1]. The averaging symbolized by the brackets, < >, in equations (1) and (12) is to be taken over the illuminated portion of the surface. For simplicity in all calculations it has been assumed that

$$\theta_0 = \theta_0^h = \theta_0^v = 0\,.\tag{16}$$

This should be an adequate approximation for the very grazing angles involved $\leq.02$ rad. The averaging brackets in this case are

$$<K_{ii}> = 2\int_{-\pi/2}^{0}da\int_{-\pi/2}^{\pi/2}d\beta\,K_{ii}(a,\beta)f(a,\beta)\sec^2 a\sec^2\beta\ :\tag{17}$$

Gaussian model.

The second model considered will be referred to as the "wedge model." The general ideas have been motivated by the observation of Kalmykov and Pustovoytenko[6] that wedge shape formations appear to

5

have significant impact on HH clutter return. The notion has been further discussed by Wetzel[7]. This notion is based on the fact that the crest angle of the Stokes' wave as the wave begins to break is[10] 120°. This corresponds to a wave slope of 30°. Thus, it will be generously assumed that the (γ, ϕ) coefficients of the Γ terms in equations (3) and (5) are meaningful for $\gamma = 30°$. As Wetzel[7] points out, the distribution of wave orientation, ϕ, could also be a delta function, as when the crests line up in a breaking zone, or could be uniformly distributed as in a well mixed sea. Results given in section 3.0 assume the latter and the brackets in this case become (recall that the averaging is over the illuminated wave surface)

$$< K_{ii} > = \frac{1}{\pi} \int_{\pi/2}^{3\pi/2} d\phi \int_0^\pi d\gamma \delta\left(\frac{\gamma - \pi}{6}\right) K_{ii}(\gamma, \phi) = \frac{1}{\pi} \int_{\pi/2}^{3\pi/2} d\phi K_{ii}\left(\frac{\pi}{6}, \phi\right) : \tag{18}$$

wedge model.

In section 3.0 some results will be given in terms of system clutter power (in dBm) versus range and some will be given in terms of the normalized radar cross section, σ°, as a function of range. In terms of path loss the normalized radar cross section is

$$\sigma^\circ(dB) = -PL(dB) + 10Log_{10}\left(\frac{(4\pi)^3 x^4}{\lambda^2 A}\right), \tag{19}$$

where

$$A = x\Delta x \sqrt{\frac{\pi}{ln2}} \phi_0 \qquad \lambda = rf \ wavelength, \tag{20}$$

and the only requirement is that a consistent set of units be used for λ, x, and A. It should further be pointed out that the vertical beam pattern has been omitted from equations (1) and (12). This impacts only the system clutter power returns given in section 3.0 at ranges ≤ 2 km.

3.0 RESULTS

Figures 2 through 12 show comparisons between the empirically founded GIT[11] model (and its extension as implemented in EREPS[12]) and the ray clutter calculations for the system parameters considered in earlier studies.[1-3] Specifically, the results are for a frequency of 9.6 GHz, a transmitter height of 25 m, a pulse width of 1.0 μs, and a 3 dB beam width of 1.2°. As in the earlier studies, environments considered are the standard atmosphere, 14- and 28-meter evaporation ducts at windspeeds of 10, 20, 30, and 40 knots. The solid curve is the GIT/EREPS result for horizontal polarization. Depending upon windspeed and grazing angle, GIT/EREPS results for vertical polarization can differ by several dB from those for horizontal polarization at x band. However, those differences are not considered significant for the present comparisons and the HH results are used as the empirical prototype in this study. The dash-double dot curves are the wedge model results for VV polarization, the dash-dot curves are the Gaussian model results for VV polarization, the dashed curves are the wedge model results for HH polarization, and the dotted curves are the Gaussian model results for HH polarization. As expected, the impact of wedge scatter on HH polarization is quite significant for all environments and wind speeds. For example, at 10 knots wedge scatter reduces the difference between vertical and horizontal clutter from about 25 dBm to about 12 dBm and at 40 knots it reduces the difference from about 17 dBm to about 12 dBm. However, in all instances the calculated horizontal returns are noticeably less than the vertical returns in contradiction with x-band measurements. Thus, although scattering from wedges may play a role, it does appear that some other scattering mechanism(s) such as foam, water spray, or droplets is also playing a role at x band. Comparisons with the GIT/EREPS curves show that in the range from about 2 to 10 km the empirical results generally agree best with the Gaussian HH polarization model at 10 knots and with the VV polarized results at the higher wind speeds. This would suggest that wedge scattering does not play a role at 10 knots but does become activated at the higher wind speeds. In the ducting cases beyond about 10 km out to 40 km, the calculations indicate a x^{-5} fall off with range rather than a x^{-3} fall off indicated by the GIT/EREPS results. The origin of this difference should be tracked down.

In the case of the standard atmosphere, the fall off with range at ranges >10 km calculated via waveguide methods (figures 14 through 17) indicate a somewhat slower fall off than the GIT/EREPS results. This is presumably because the GIT/EREPS curves assume a fall off of $x^{-3}\exp(-\alpha x)$ with α being the attenuation rate of the least attenuated mode. However, the waveguide result in this case indicates a fall off of $x^{-1}\exp(-\alpha x)$.

A complete set of waveguide results for the ducting cases are not given because in their region of validity they agree with the ray results. However, representative comparisons for the normalized radar cross section versus range are shown in figures 18 and 19. The results apply to the 14- and 28-m ducts with a wind speed of 20 knots. The solid curves are the waveguide results for VV polarization, the dash-dot curves are the ray results for VV polarization, the dotted curves are the waveguide results for HH polarization, and the dashed curves are the ray results for HH polarization. The waveguide results break down at about 5 km. However, as mentioned above, the agreement with ray calculations out to 40 km is quite good.

Figures 20 through 22 represent an alternative display of the previous results. In particular they show the normalized radar cross section for the Gaussian model as a function of range with windspeed as a parameter. The solid curves are for VV polarization and the dashed curves are for HH

polarization. Figure 20 is for the standard atmosphere and shows ray results at ranges less than about 10 km and waveguide results beyond there. Figure 21 applies to the 14-m duct and figure 22 to the 28-m duct, and in both cases only the ray results are shown. Wetzel[7] has quoted −40 dB as a consensus measure of the normalized cross section corresponding to a one degree grazing angle (i.e., at a range of ≃1.4 km). Generally, the HH results are below this figure and the VV results above it. The figures clearly illustrate a much stronger wind dependence for HH polarization than for VV polarization. As expected, it will also be seen that the normalized cross section fall off with range beyond about 20 km is larger for the 14-m duct than for the 28-m duct.

Figures 23 through 25 show the normalized cross section for the wedge model as a function of range with wind speed as a parameter. The legend for the curves is the same as for figures 20 through 22. Figure 23 is for the standard atmosphere and shows ray results at ranges less than about 10 km and waveguide results beyond there. Not surprisingly, the results corresponding to one degree grazing angle (i.e., a range of ≃1.4 km) are high compared with the consensus measurement of −40 dB quoted by Wetzel[7]. In this instance the wind speed dependence is the same for both the HH and VV polarizations and comes entirely from the wind speed dependence of the sea spectrum. As before, the fall off of the normalized cross section with range beyond about 20 km is greater for the 14-m duct than for the 28-m duct.

8

4.0 DISCUSSION

Surface normal tilting perpendicular to the unperturbed plane of incidence has the effect that an incident horizontally (vertically) polarized wave presents both polarization types to the scattering facet. Thus, for such a surface, backscatter, even for a horizontally or vertically polarized incident wave, results from incidence of both polarizations on the locally perturbed surface. The effect was first treated by Valenzuela[3]. In this study, methods described by Ulaby et al.[9] have been used for the analysis. This led to minor modifications of Valenzuela's formulas. It is believed that the coefficients, K_{ii}, used in this study are, unlike Valenzuela's coefficients, correct to all orders in the tilt angles. As pointed out in section 2.0, there is an inconsistency in coupling these higher order effects with first order Bragg scattering theory. License to do so has been taken and the wedge model results do invoke that license. Results based on the Gaussian model, however, should be totally valid within the spirit of the composite model, since the rms tilt angles are ≤ 0.2 rad.

Both the wedge and Gaussian models assume well mixed seas. In the Gaussian model, the tilt angle distribution in and perpendicular to the unperturbed plane of incidence has been assumed to be Gaussian distributed with equal variance in all directions. In the wedge model, the angle between the local surface normal and the unperturbed surface normal has been taken to be 30° which is appropriate for a Stokes' wave just before breaking. In the wedge model, the azimuthal distribution has been taken to be symmetric.

Clutter power returns as a function of range shown in figures 2 through 12 point out that the impact of wedge scatter is much more significant for HH scatter than for VV scatter. For example, at 10 knots wedge scatter reduces the difference between the HH and VV returns from about 25 dBm to about 12 dBm and at 40 knots reduces the difference from about 17 dBm to about 12 dBm. However, in all instances the horizontal returns are noticeably less than the vertical returns. This is contrary to measurement. For example, figure 26 taken from the recent work of Chan[13] shows the normalized cross section, $\sigma°$, in dB as a function of grazing angle at x band for sea state 2. For grazing angles $\simeq 1°$, the magnitude of $\sigma°$ is similar for both polarizations. For reference, the 120° (30°) azimuths were identified as the upswell (cross-swell) directions. The situation at s band is quite different as figure 27 shows (Chan[13]). For example, for an azimuth of 30° the differences between vertical and horizontal polarization exceed 15 dB. Results, not given in this paper, for an s band frequency indicate that the theoretical differences between HH and VV return are comparable to the calculated x-band differences. Thus, one of many challenges is to account for these s- and x-band differences. It certainly does seem that the scattering mechanisms are quite different in the two regimes. In particular, Chan[13] has suggested that the x-band results are strongly influenced by water spray and droplets. Wetzel[7] and Long[14] have suggested still other mechanisms. Whatever the truth may be, it is likely that these other mechanisms could be incorporated into the propagators developed in the earlier studies. Another obvious point of interest which follows from Chan's[13] results is the azimuthal look direction-dependence. As pointed out by Wetzel[7], clutter return associated with lining up of wedge crests (as in a breaking zone) could also be calculated following the present methods, but that has not been done in this study. Wetzel's[7] estimates of the effect would indicate no major dependence until the look angle approaches the cross-swell direction.

Returning to the x-band results given in figures 2 through 12, it will be seen that comparisons with the GIT/EREPS curves show that in the range from about 2 to 10 km the empirical results generally

agree best with the Gaussian HH polarization model at 10 knots and with the VV results at the higher wind speeds. In the ducting cases beyond about 10 km, the calculations indicate over the 40-km range a x^{-5} fall off with range rather than a x^{-3} fall off indicated by the GIT/EREPS results. The origin of this difference should be tracked down.

Figures 20 through 25 represent an alternative display of results presented earlier in the study. In particular, they show the normalized cross section as a function of range with wind speed as a parameter. Wetzel[7] has quoted −40 dB as a consensus measure of the normalized cross section corresponding to a one degree grazing angle (i.e., at a range of ≈1.4 km). In the case of the Gaussian model, the HH results are below this figure and the VV results above it. In the case of the wedge model the results are high compared with the −40 dB consensus value.

Suggested work for the future would include

a. An understanding of the physical origin of the difference between HH and VV polarization returns predicted by first order Bragg scatter.

b. Effect of the line up of wedge crests as contrasted with the azimuthal symmetry assumption used in the present wedge model.

c. Influence of additional scattering mechanisms such as foam, water spray, and droplets as a function of frequency and wind speed.

d. Calculation of depolarization (i.e., HV and VH) cross sections. This can be done using the present methods.

e. *Additional frequency and range calculations and comparisons with pe results*. Resolution, for example, of the differences between s- and x-band backscatter.

f. Origin of the discrepancy between the range dependence calculated from the models and the GIT/EREPS predictions.

g. Additional backscatter measurements at low grazing angles ≤1° as a function of frequency, windspeed, and refractivity environment.

h. General computer program which integrates the component parts of the path loss formulas. For example, in this study the $<K_{ii}>$ were determined by separate averaging algorithms. Those could be integrated into existing codes*.

---

* The following unpublished internal NOSC documents were used as references. For further information, please contact author.
Pappert, R.A. and L.R. Hitney. "Changes and Additions to "MLAYER" to Accommodate Sea Surface Backscatter."
Pappert, R.A. and L.R. Hitney. "A Test Ray Trace Program for Backscatter in Evaporation Ducts."

5.0 REFERENCES

1. Pappert, R. A. 1989. "Radar Clutter Via Waveguide Methods." NOSC TD 1739 (Dec). Naval Ocean Systems Center, San Diego, CA.

2. Pappert, R. A. 1990. "Radar Clutter Via Ray Methods." NOSC TD 1809 (May). Naval Ocean Systems Center, San Diego, CA.

3. Valenzuela, G. R. 1968. "Scattering of Electromagnetic Waves from a Tilted Slightly Rough Surface," *Radio Science*, vol. 3, no. 11, pp. 1057–1066.

4. Valenzuela, G. R. 1978. "Theories for the Interaction of Electromagnetic and Oceanic Waves—A Review," *Boundary-Layer Meteorology*, vol. 13, pp. 61–85.

5. Pierson, W. J. 1976. "The Theory and Applications of Ocean Wave Measuring Systems at and Below Sea Surface on the Land, from Aircraft and from Space Craft," NASA CR-2646, National Aeronautics and Space Administration, Washington, DC.

6. Kalmykov, A. I. and V. V. Pustovoytenko. 1976. "On Polarization Features of Radio Signals Scattered from the Sea Surface at small Grazing Angles," *Jour. Geophys. Res.*, vol. 81, pp. 1960–1964.

7. Wetzel, L. B. 1987. "Models for Electromagnetic Scattering from the Sea at Extremely Low Grazing Angles." NRL Memorandum Report 6098.

8. Hitney, H. V. 1988. "Evaporation Duct Effects on Low Altitude Propagation." NOSC TR 1304 (Jun). Naval Ocean Systems Center, San Diego, CA.

9. Ulaby, F. T., R. K. Moore, and A. K. Fung. 1982. *Microwave Remote Sensing Active and Passive, Vol. II: Radar Remote Sensing and Surface Scattering and Emission Theory*, Addison-Wesley Publishing Co., London.

10. Kinsman, B. 1965. *Wind Waves: Their Generation and Propagation on the Ocean Surface*, Prentice-Hall, Inc., Englewood Cliffs, NJ.

11. Horst, M. M., F. B. Dyer, and M. T. Tuley. 1978. "Radar Sea Clutter Model," *Proc. IEEE, International Conference on Antennas and Propagation*, (pp. 6–10). London.

12. Patterson, W. L., C. P. Hattan, H. V. Hitney, R. A. Paulus, A. E. Barrios, G. E. Lindem, and K. D. Anderson. 1990. "Engineer's Refractive Effects Prediction System (EREPS Revision 2.0)." NOSC TD 1342 (Feb). Naval Ocean Systems Center, San Diego, CA.

13. Chan, H. C. 1990. "Radar Sea Clutter at Low Grazing Angles," *IEEE Proceedings*, 137 Part F, vol. 2, pp. 102–112.

14. Long, M. W. 1974. "On a Two Scatterer Theory of Sea Echo," *IEEE Trans.*, AP 22, vol. 5, pp. 667–672.
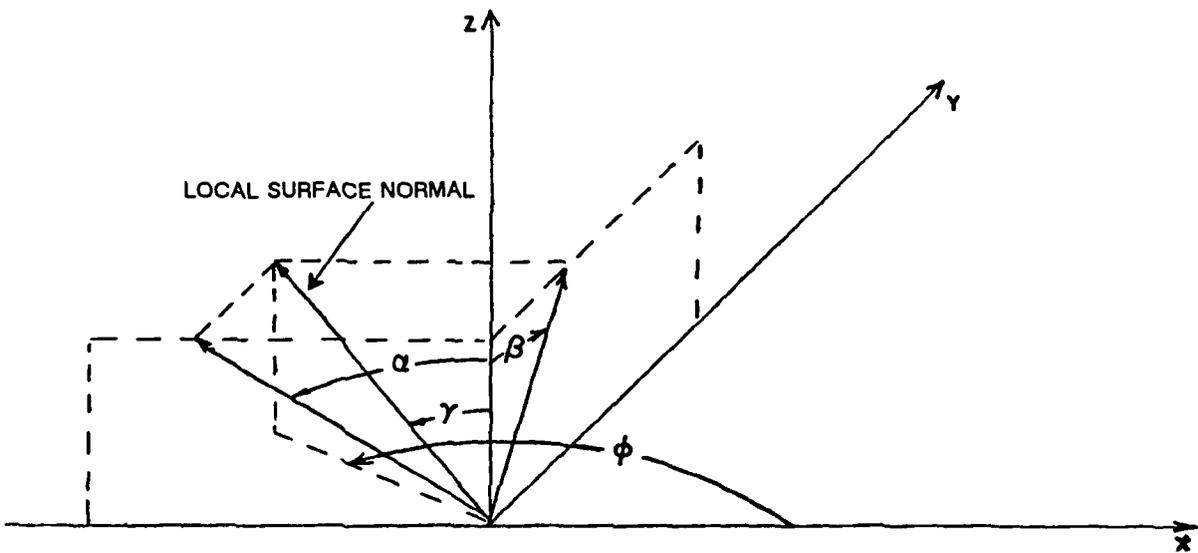
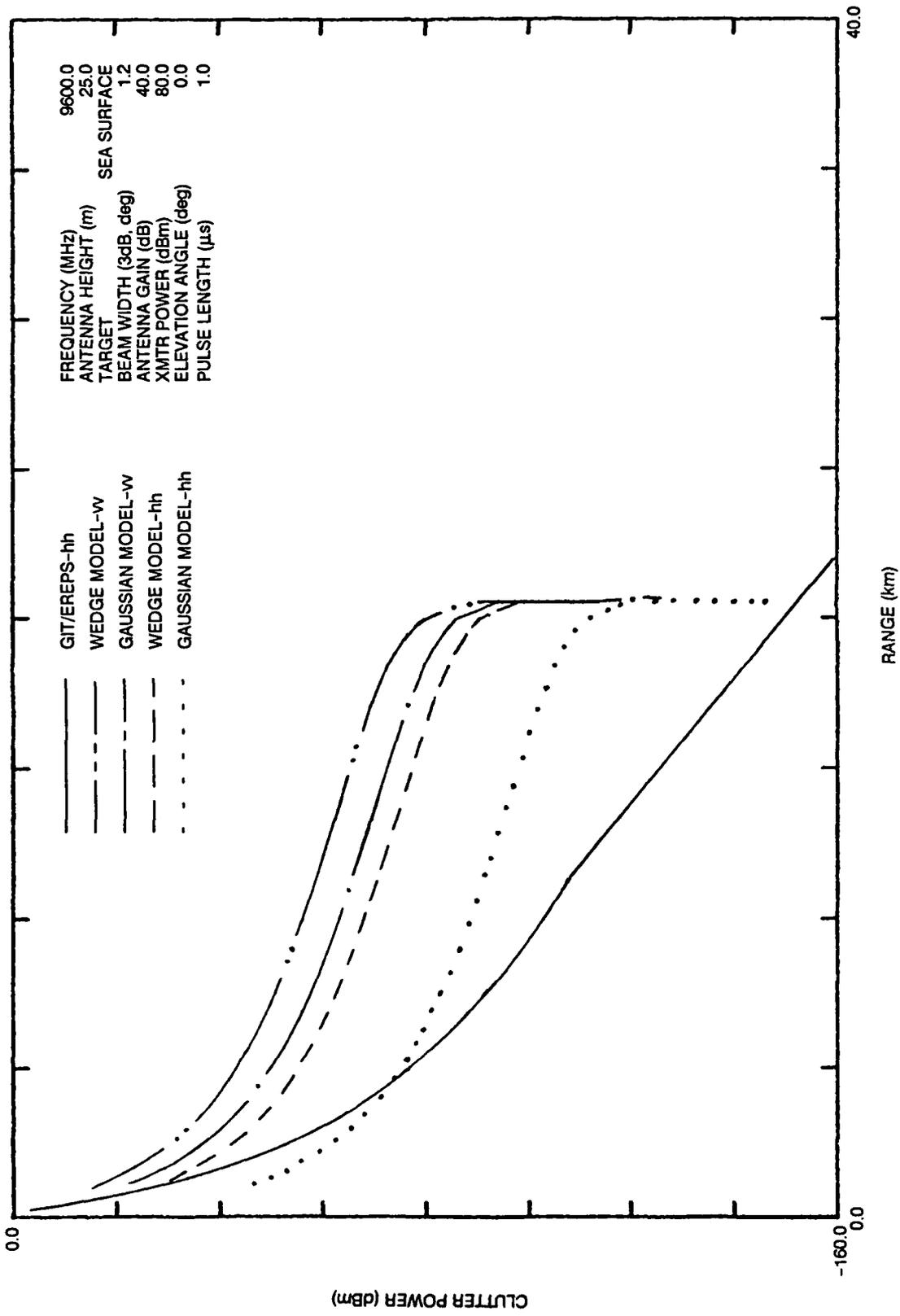Figure 1. Decomposition of the local surface normal.

12

Figure 2. Clutter power versus range. GIT/EREPS comparisons with ray models. Standard atmosphere with 10-knot wind.

13

FREQUENCY (MHz)	9600.0	
ANTENNA HEIGHT (m)	25.0	
TARGET	SEA SURFACE	
BEAM WIDTH (3dB, deg)	1.2	
ANTENNA GAIN (dB)	40.0	
XMTR POWER (dBm)	80.0	
ELEVATION ANGLE (deg)	0.0	
PULSE LENGTH (µs)	1.0	

GIT/EREPS-hh

WEDGE MODEL-vv

GAUSSIAN MODEL-vv

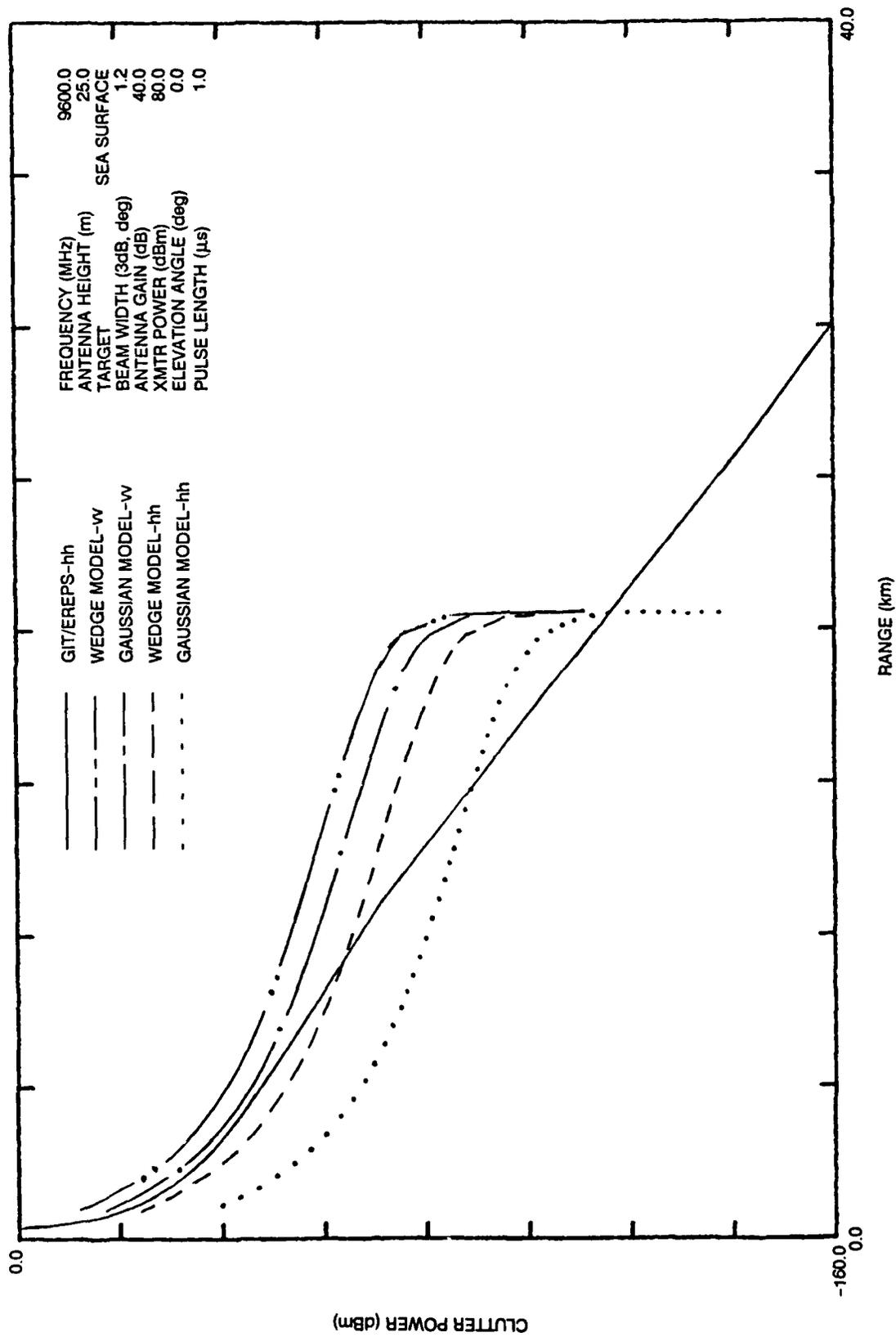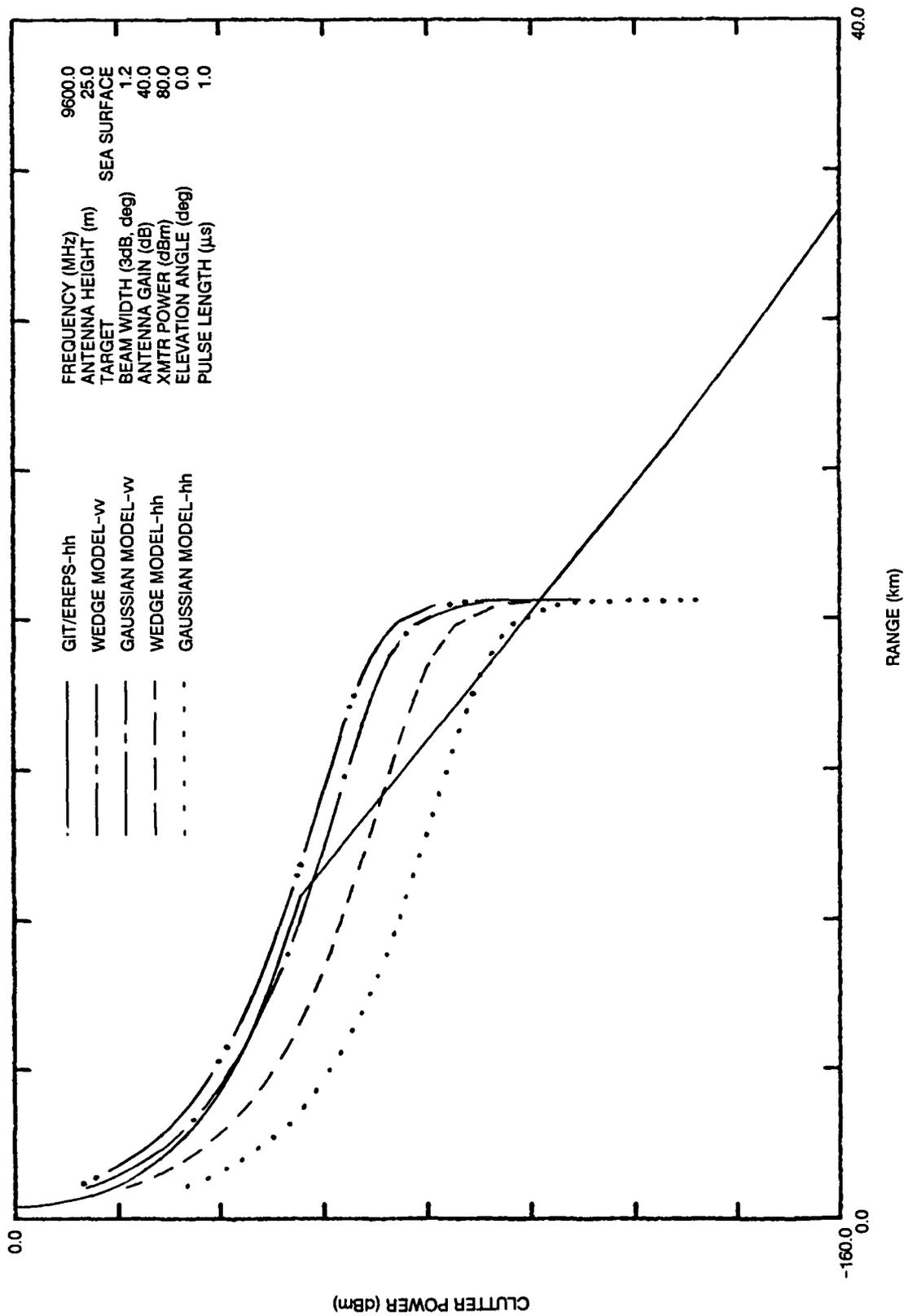WEDGE MODEL-hh

GAUSSIAN MODEL-hh

Figure 3. Clutter power versus range. GIT/EREPS comparisons with ray models. Standard atmosphere with 20-knot wind.

14

Figure 4. Clutter power versus range. GIT/EREPS comparisons with ray models. Standard atmosphere with 30-knot wind.
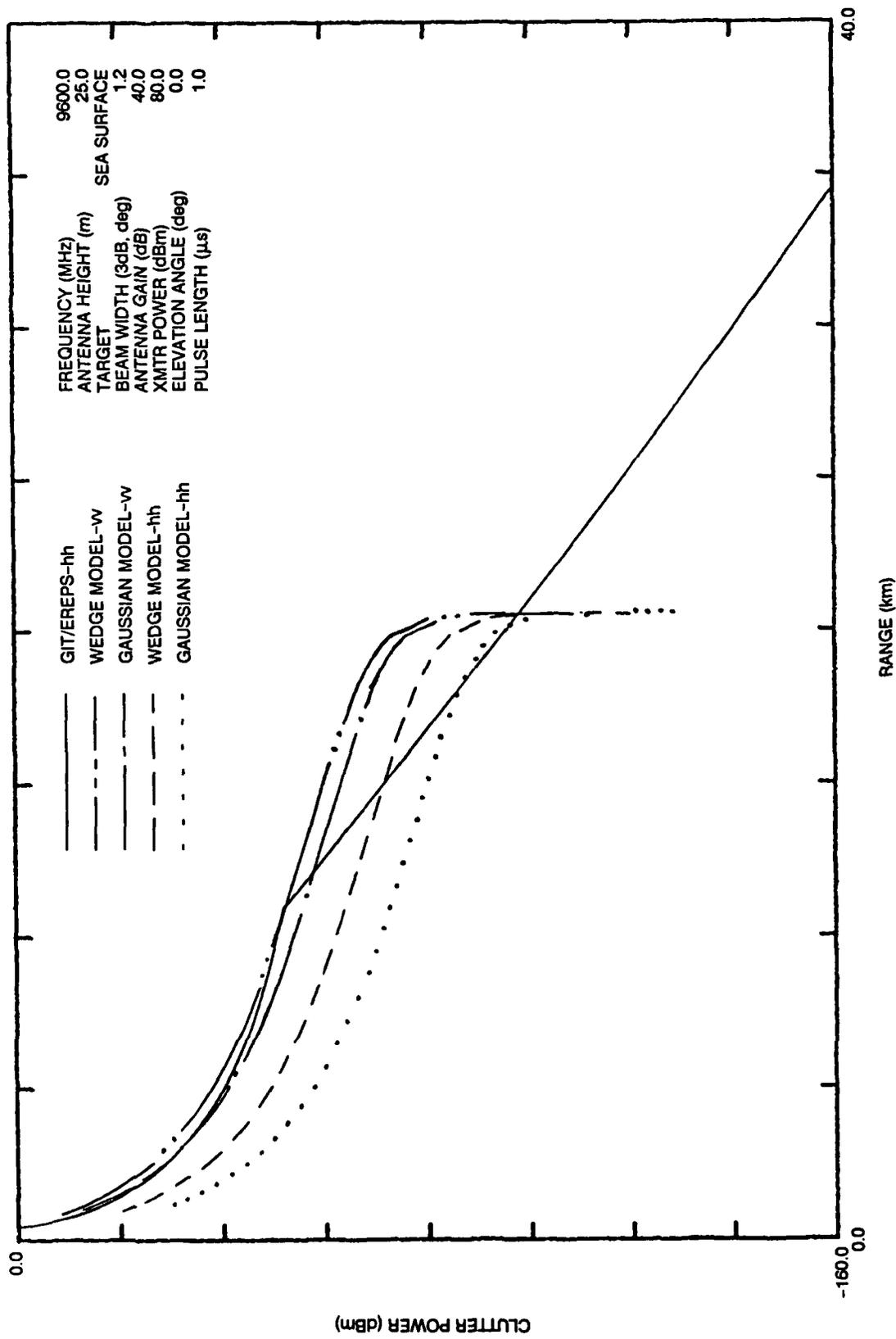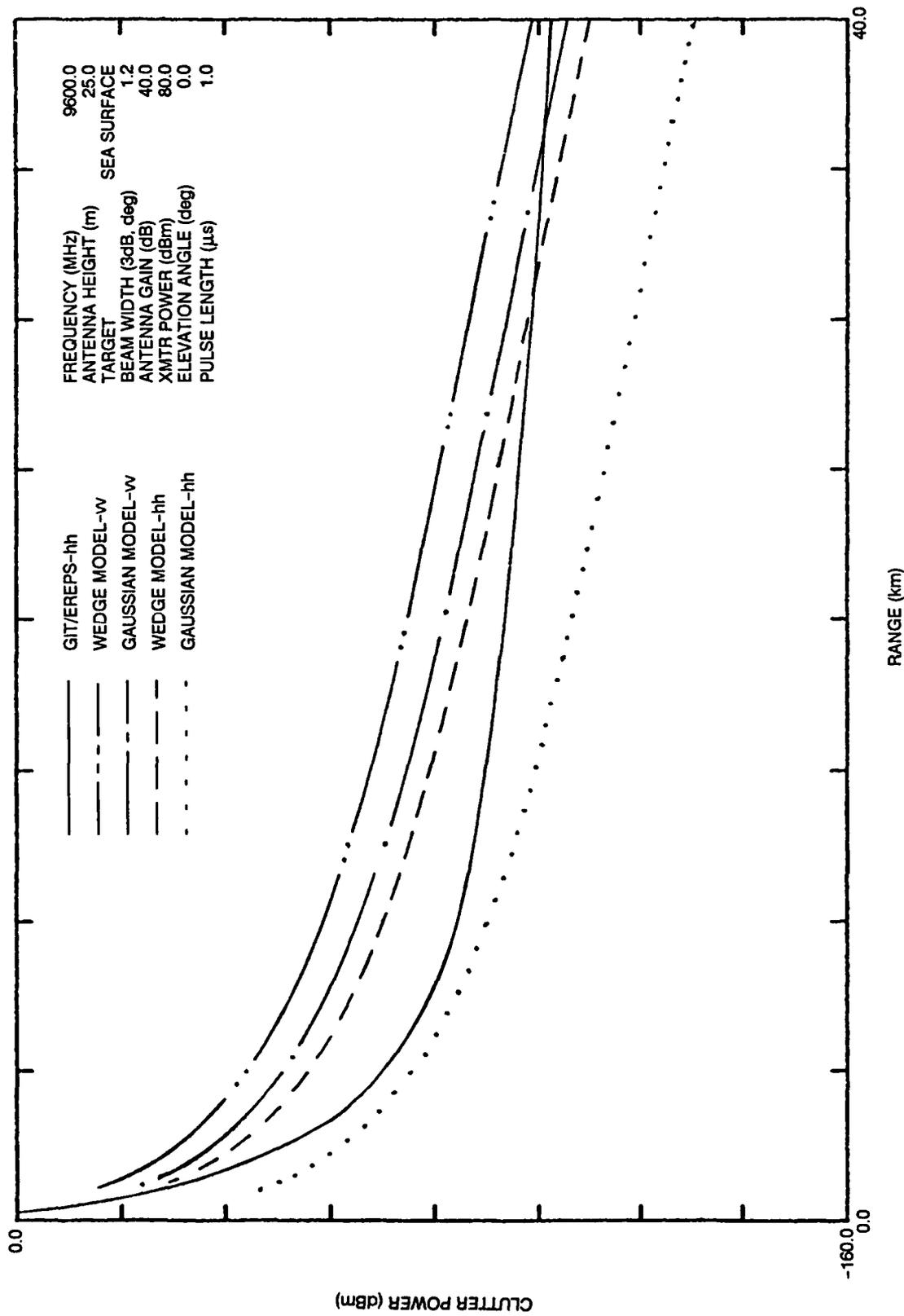
15

FREQUENCY (MHz)	9600.0
ANTENNA HEIGHT (m)	25.0
TARGET	SEA SURFACE
BEAM WIDTH (3dB, deg)	1.2
ANTENNA GAIN (dB)	40.0
XMTR POWER (dBm)	80.0
ELEVATION ANGLE (deg)	0.0
PULSE LENGTH (µs)	1.0

GIT/EREPS-hh

WEDGE MODEL-vv

GAUSSIAN MODEL-vv

WEDGE MODEL-hh

GAUSSIAN MODEL-hh

Figure 5. Clutter power versus range. GIT/EREPS comparisons with ray models. Standard atmosphere with 40-knot wind.

16

FREQUENCY (MHz)	9600.0	
ANTENNA HEIGHT (m)	25.0	
TARGET	SEA SURFACE	
BEAM WIDTH (3dB, deg)	1.2	
ANTENNA GAIN (dB)	40.0	
XMTR POWER (dBm)	80.0	
ELEVATION ANGLE (deg)	0.0	
PULSE LENGTH (µs)	1.0	

GIT/EREPS-hh
WEDGE MODEL-vv
GAUSSIAN MODEL-vv
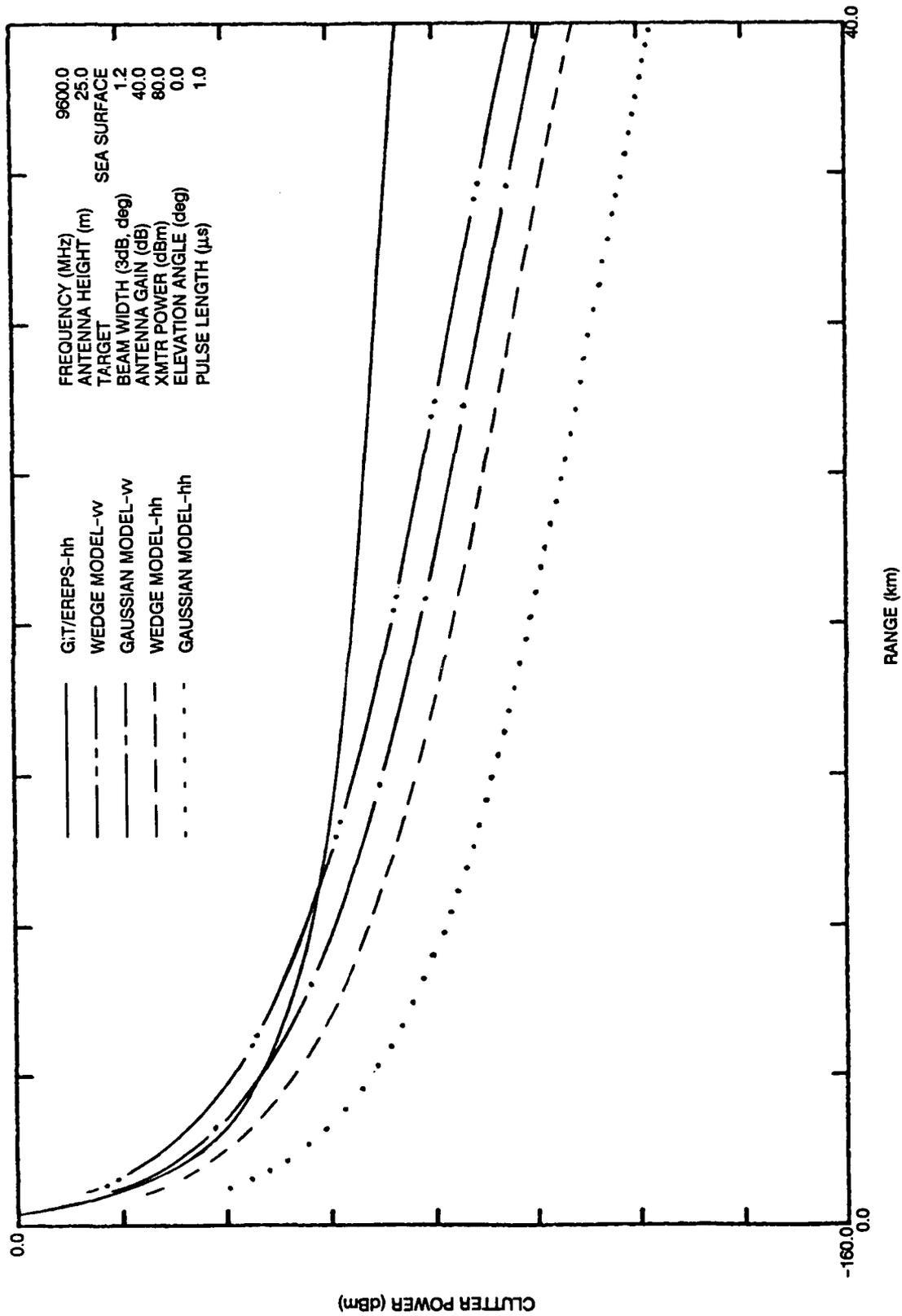WEDGE MODEL-hh
GAUSSIAN MODEL-hh

Figure 6. Clutter power versus range. GIT/EREPS comparisons with ray models. Fourteen-meter duct with 10-knot wind

Figure 7. Clutter power versus range. GIT/EREPS comparisons with ray models. Fourteen-meter duct with 20-knot wind
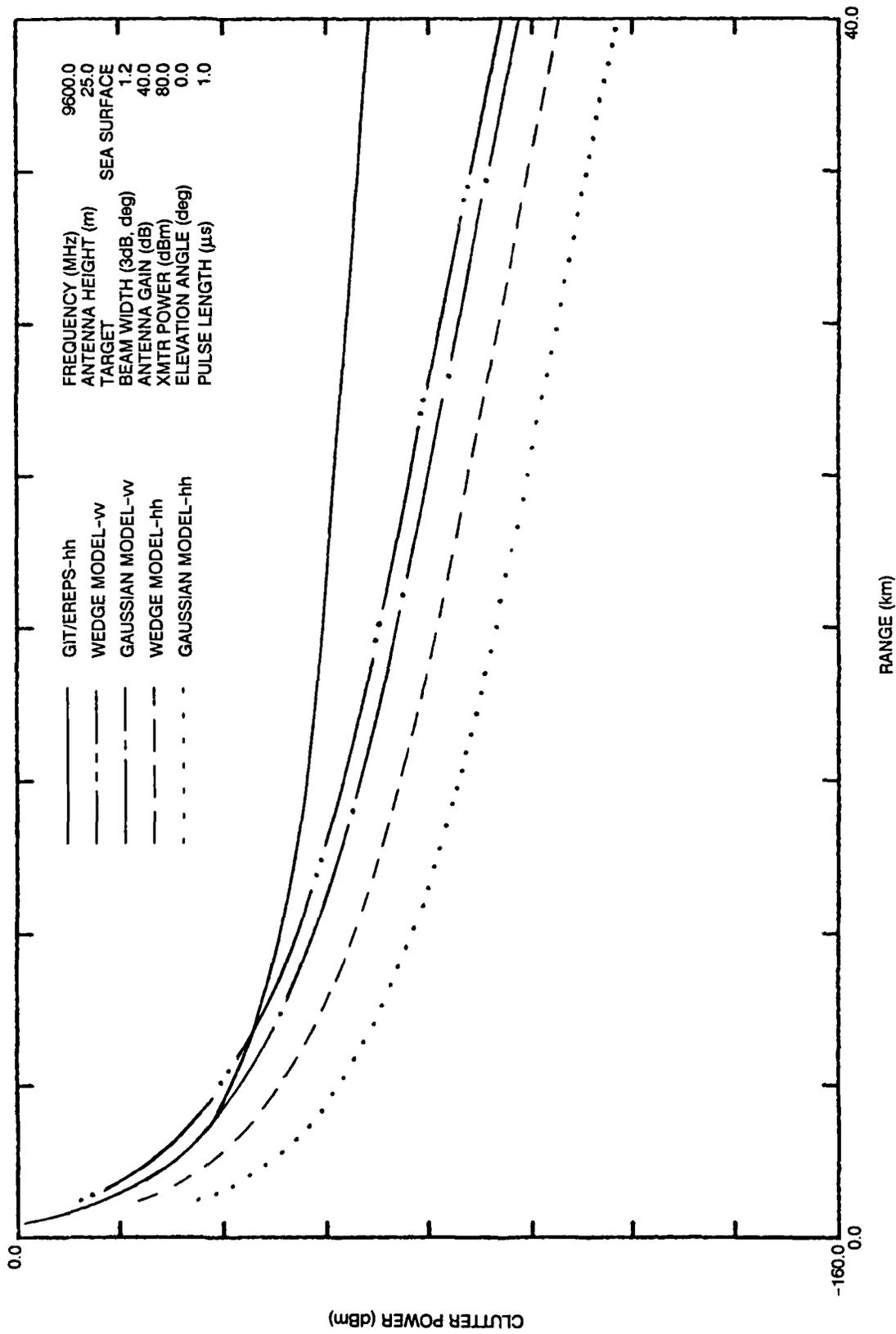
18

Figure 8. Clutter power versus range. GIT/EREPS comparisons with ray models. Fourteen-meter duct with 30-knot wind
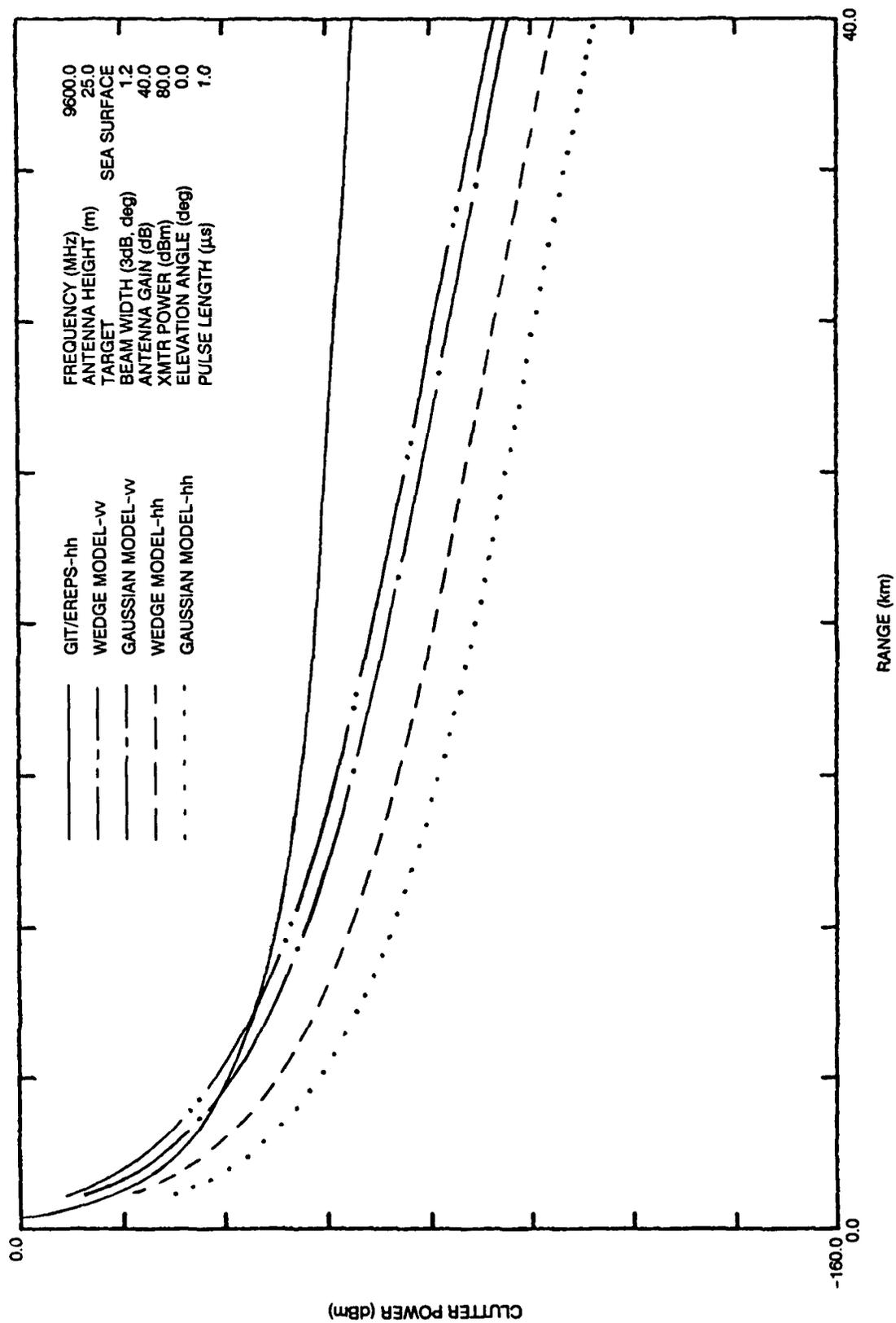
19

Figure 9. Clutter power versus range. GIT/EREPS comparisons with ray models. Fourteen-meter duct with 40-knot wind
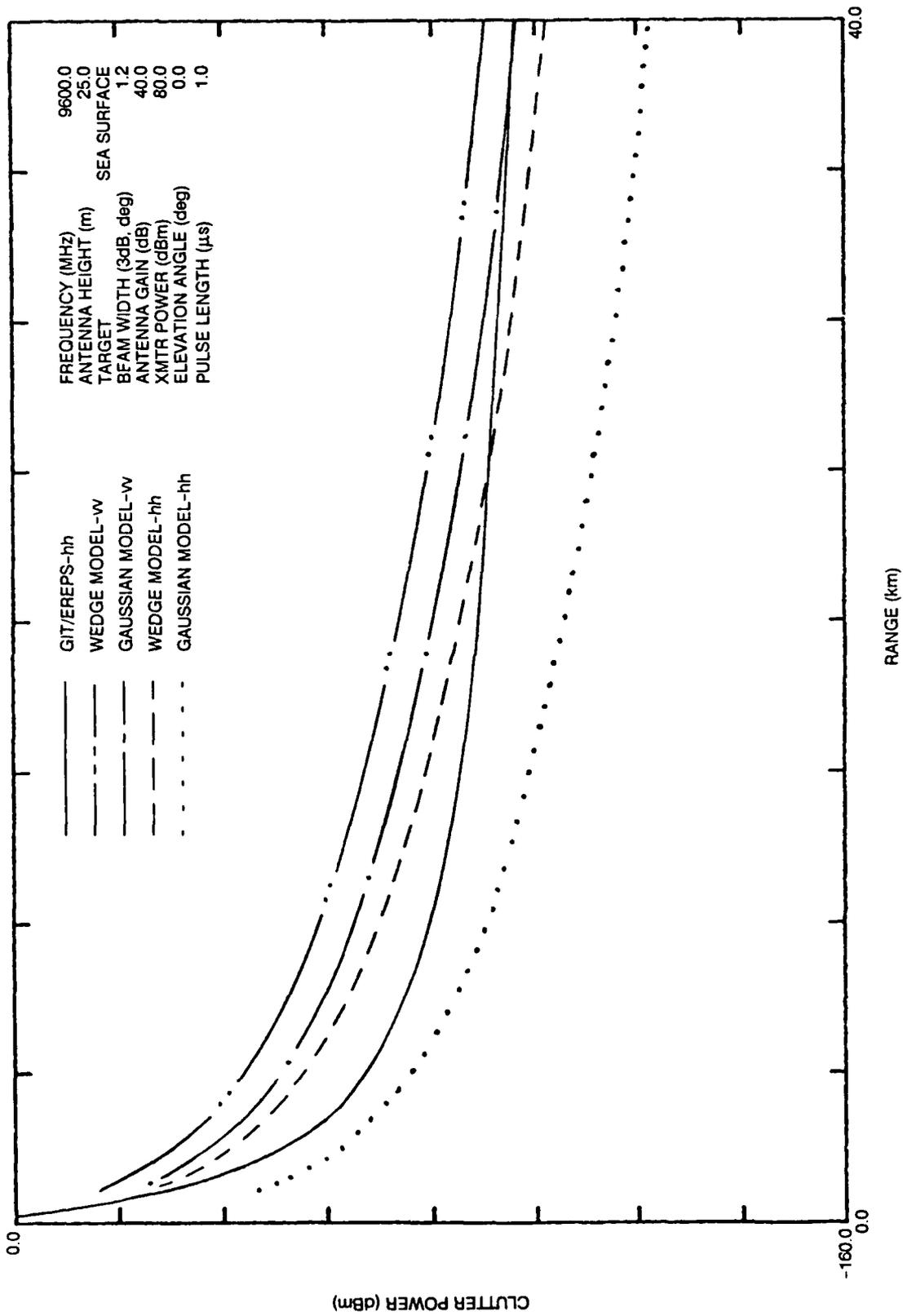
Figure 10. Clutter power versus range. GIT/EREPS comparisons with ray models. Twenty-eight-meter duct with 10-knot wind

21

FREQUENCY (MHz)	9600.0
ANTENNA HEIGHT (m)	25.0
TARGET	S±∼ SURFACE
BEAM WIDTH (3dB, deg)	1.2
ANTENNA GAIN (dB)	40.0
XMTR POWER (dBm)	80.0
ELEVATION ANGLE (deg)	0.0
PULSE LENGTH (µs)	1.0

GIT/EREPS-hh
WEDGE MODEL-vv
GAUSSIAN MODEL-vv
WEDGE MODEL-hh
GAUSSIAN MODEL-hh
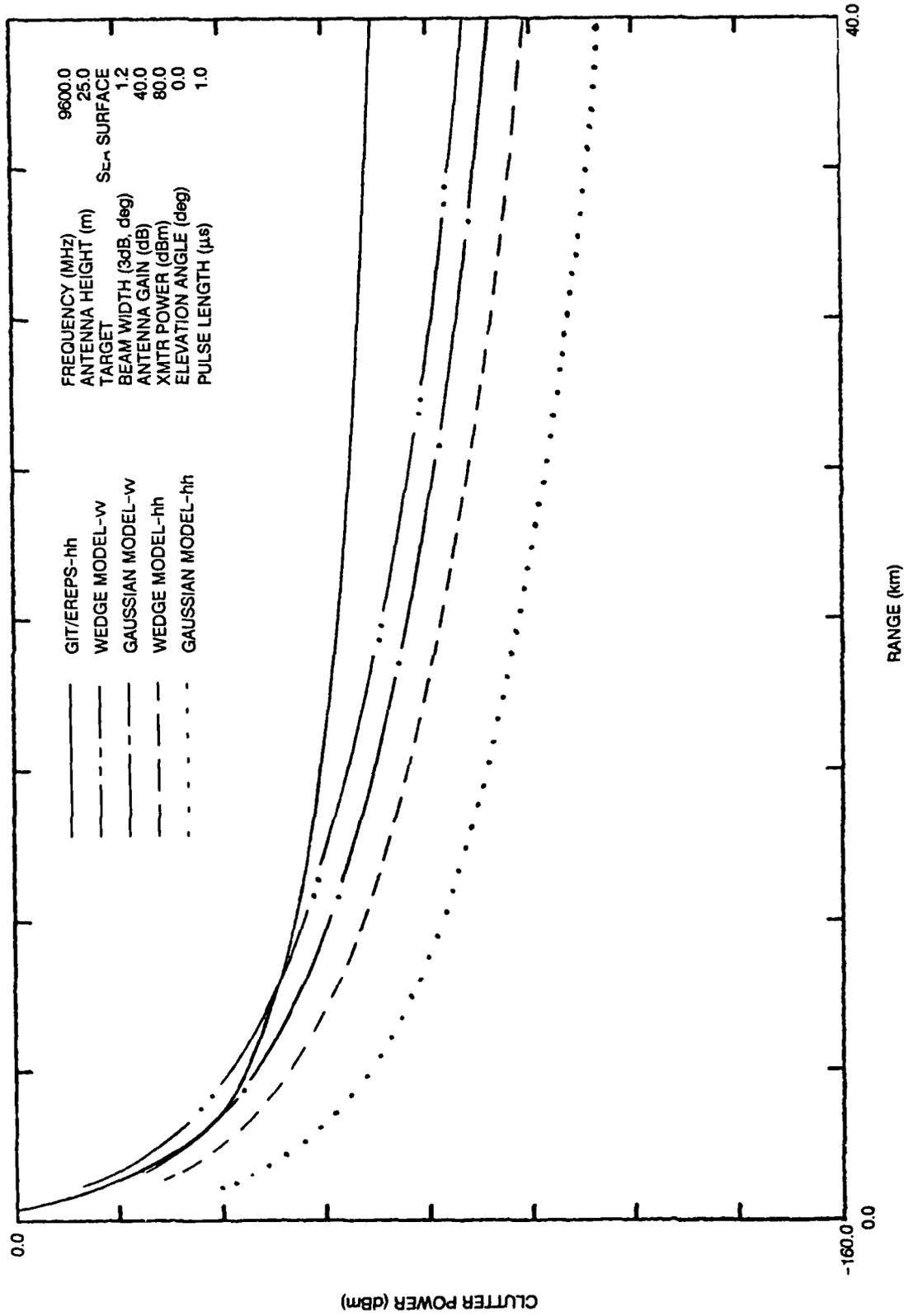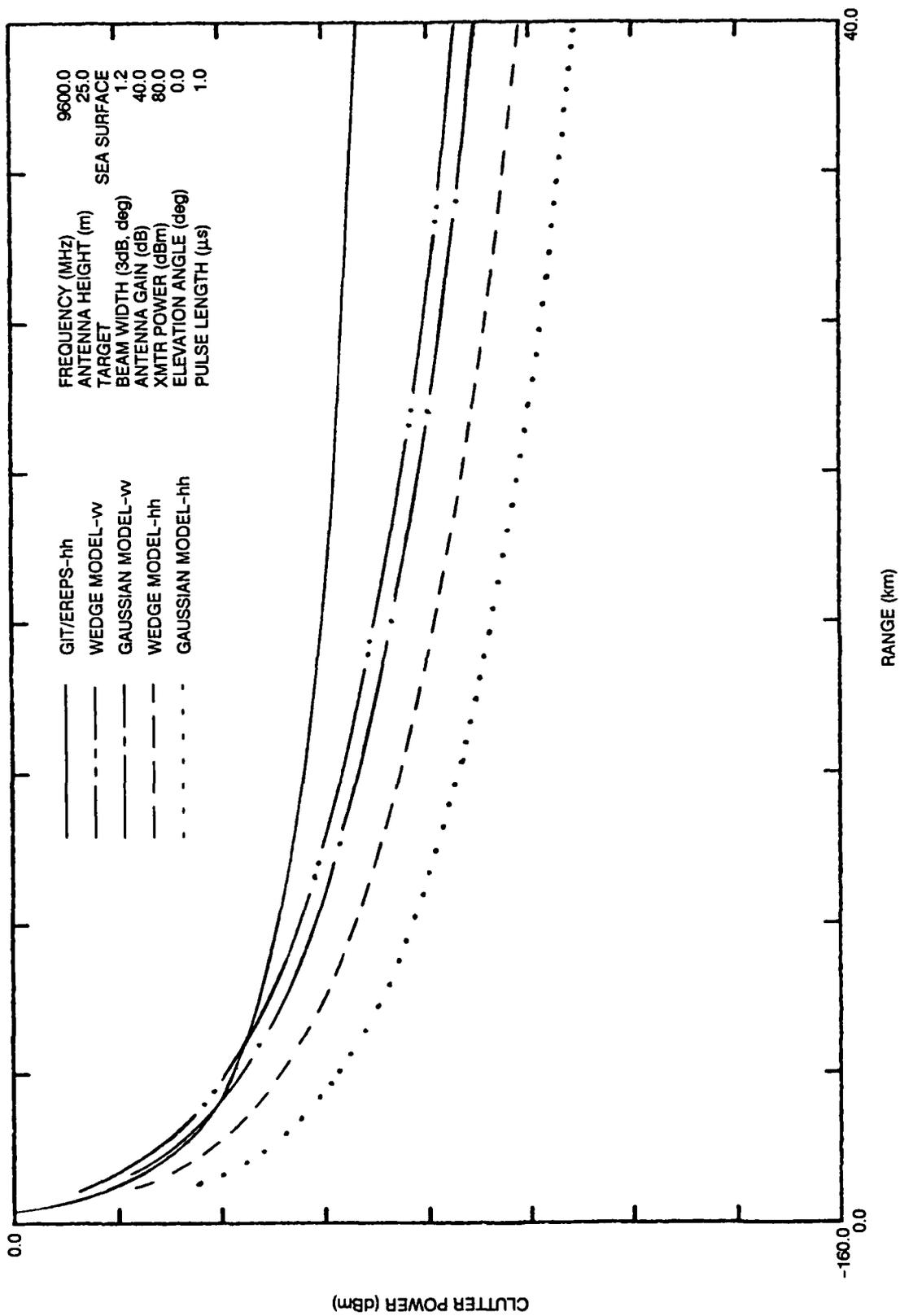
RANGE (km)

CLUTTER POWER (dBm)

Figure 11. Clutter power versus range. GIT/EREPS comparisons with ray models. Twenty-eight-meter duct with 20-knot wind

22

Figure 12. Clutter power versus range. GIT/EREPS comparisons with ray models. Twenty-eight-meter duct with 30-knot wind

23

gg

FREQUENCY (MHz) 9600.0
ANTENNA HEIGHT (m) 25.0
TARGET SEA SURFACE
BEAM WIDTH (3dB, deg) 1.2
ANTENNA GAIN (dB) 40.0
XMTR POWER (dBm) 80.0
ELEVATION ANGLE (deg) 0.0
PULSE LENGTH (µs) 1.0

GIT/EREPS-hh
WEDGE MODEL-vv
GAUSSIAN MODEL-vv
WEDGE MODEL-hh
GAUSSIAN MODEL-hh

CLUTTER POWER (dBm)

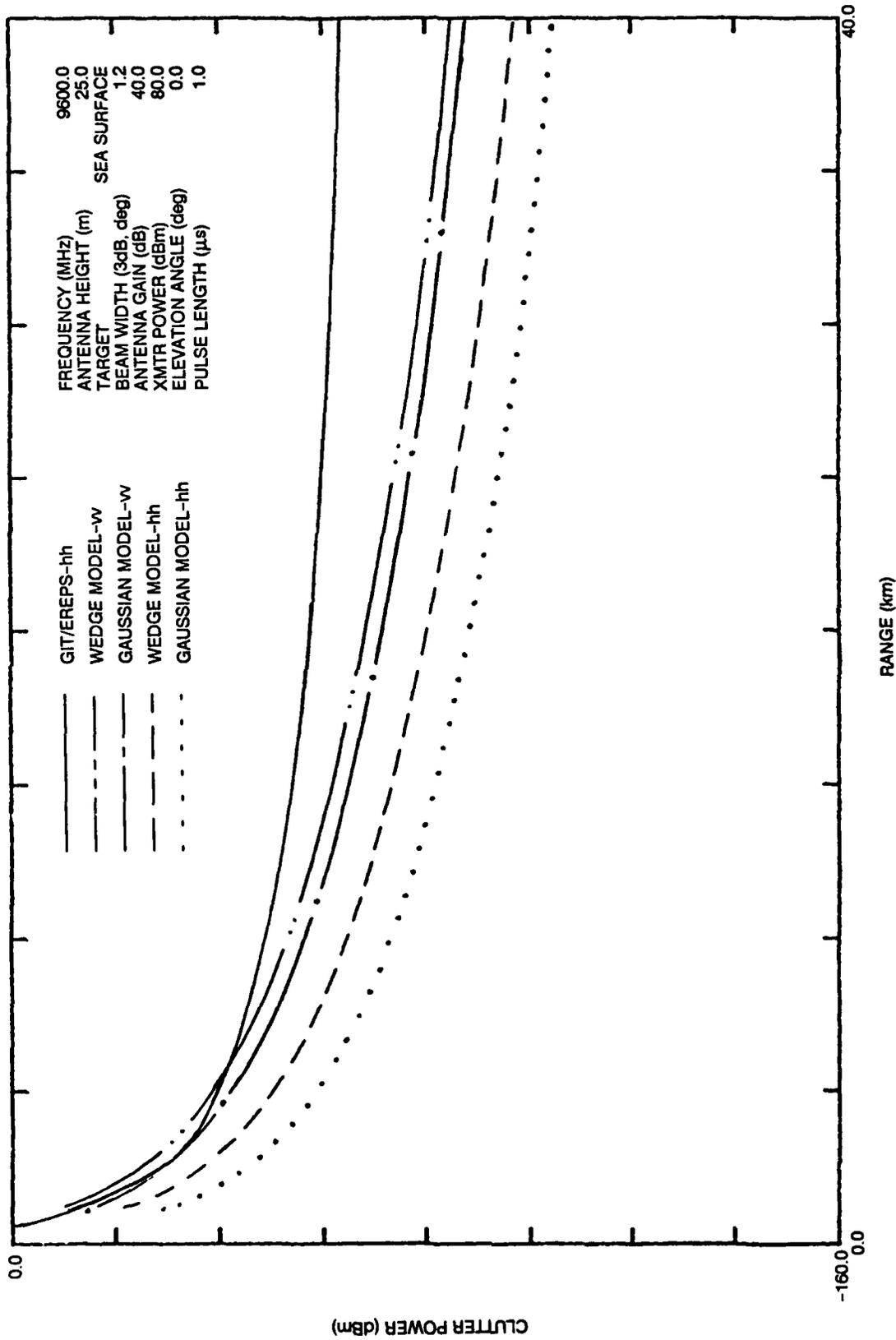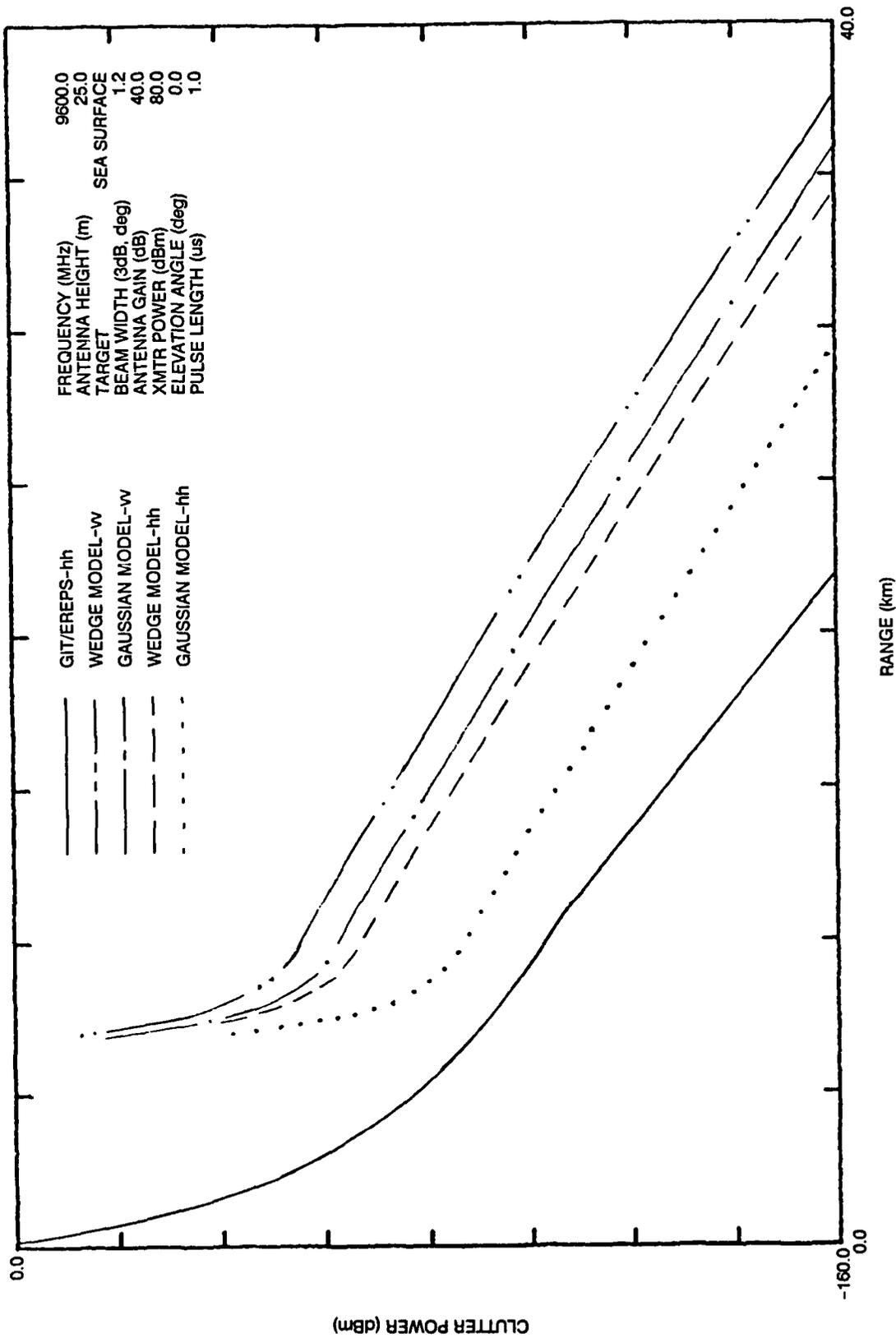0.0

-160.0

0.0   RANGE (km)   40.0

Figure 13. Clutter power versus range. GIT/EREPS comparisons with ray models. Twenty-eight-meter duct with 40-knot wind

24

Figure 14. Clutter power versus range. GIT/EREPS comparisons with waveguide models. Standard atmosphere with 10-knot wind.
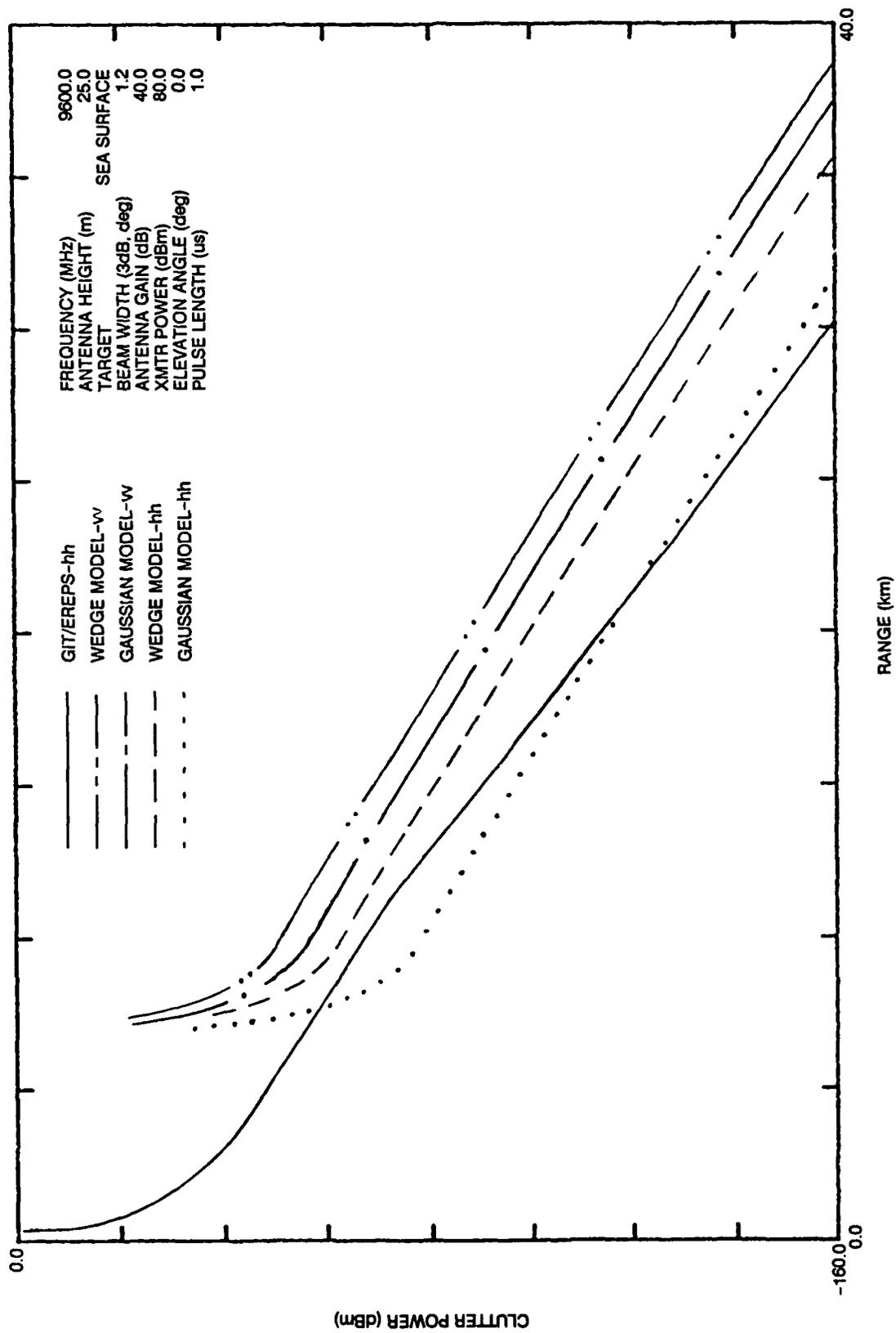
FREQUENCY (MHz)	9600.0
ANTENNA HEIGHT (m)	25.0
TARGET	SEA SURFACE
BEAM WIDTH (3dB, deg)	1.2
ANTENNA GAIN (dB)	40.0
XMTR POWER (dBm)	80.0
ELEVATION ANGLE (deg)	0.0
PULSE LENGTH (us)	1.0

GIT/EREPS-hh
WEDGE MODEL-vv
GAUSSIAN MODEL-vv
WEDGE MODEL-hh
GAUSSIAN MODEL-hh
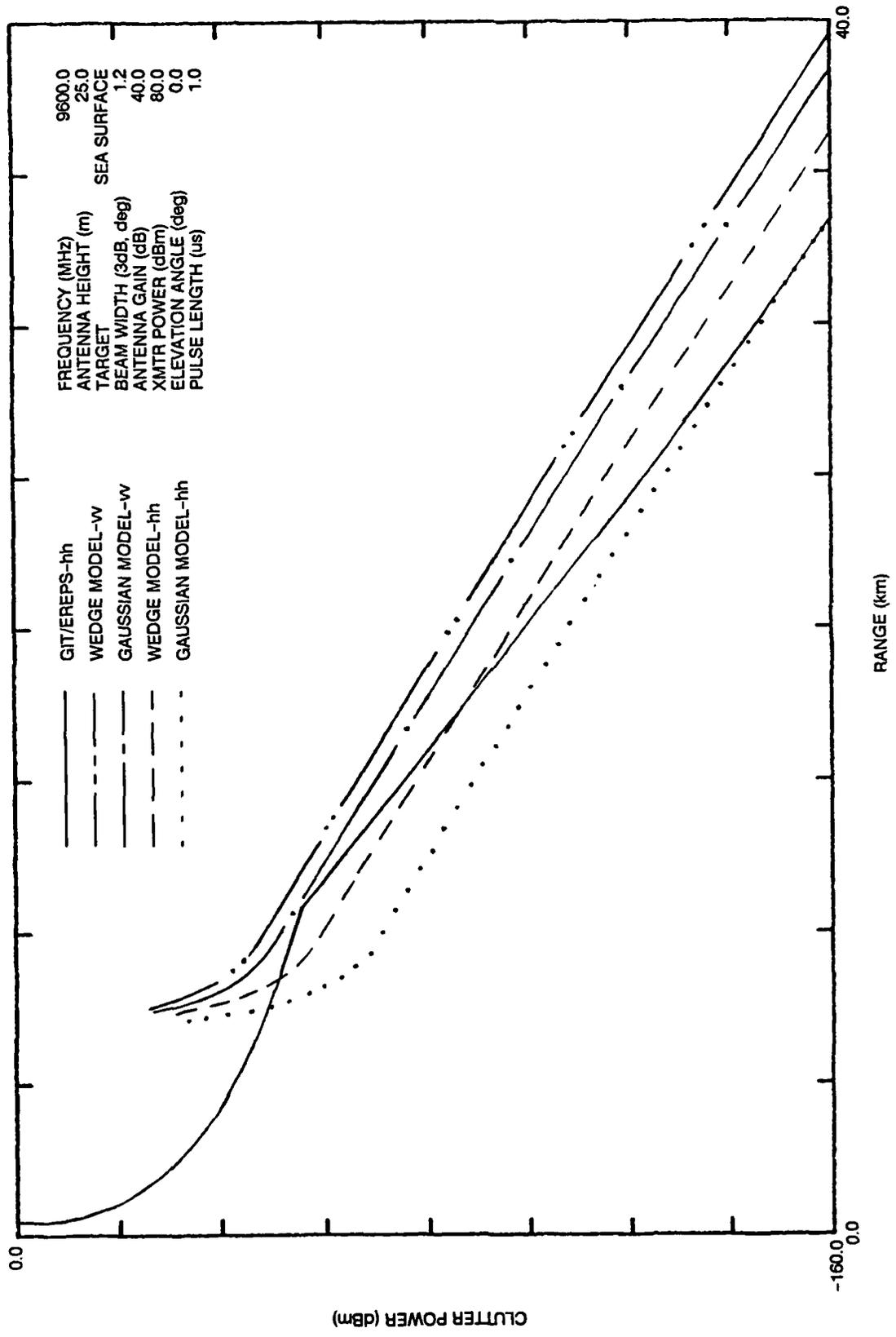
RANGE (km)

CLUTTER POWER (dBm)

Figure 15. Clutter power versus range. GIT/EREPS comparisons with waveguide models. Standard atmosphere with 20-knot wind.

26

Figure 16. Clutter power versus range. GIT/EREPS comparisons with waveguide models. Standard atmosphere with 30-knot wind.
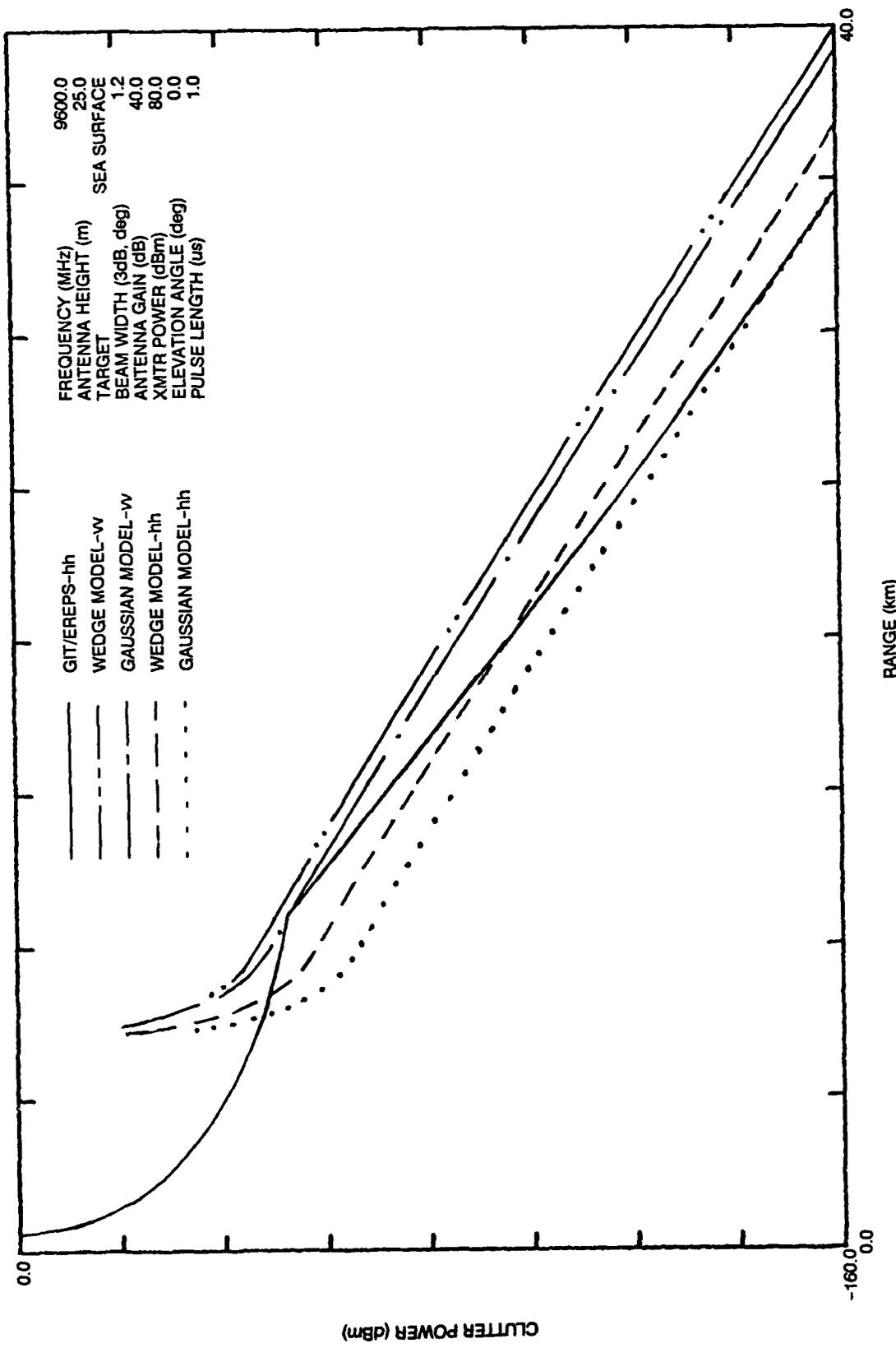
FREQUENCY (MHz)		9600.0
ANTENNA HEIGHT (m)		25.0
TARGET		SEA SURFACE
BEAM WIDTH (3dB, deg)		1.2
ANTENNA GAIN (dB)		40.0
XMTR POWER (dBm)		80.0
ELEVATION ANGLE (deg)		0.0
PULSE LENGTH (us)		1.0

GIT/EREPS-hh
WEDGE MODEL–vv
GAUSSIAN MODEL–vv
WEDGE MODEL–hh
GAUSSIAN MODEL–hh

RANGE (km)

CLUTTER POWER (dBm)

Figure 17. Clutter power versus range. GIT/EREPS comparisons with waveguide models. Standard atmosphere with 40-knot wind.
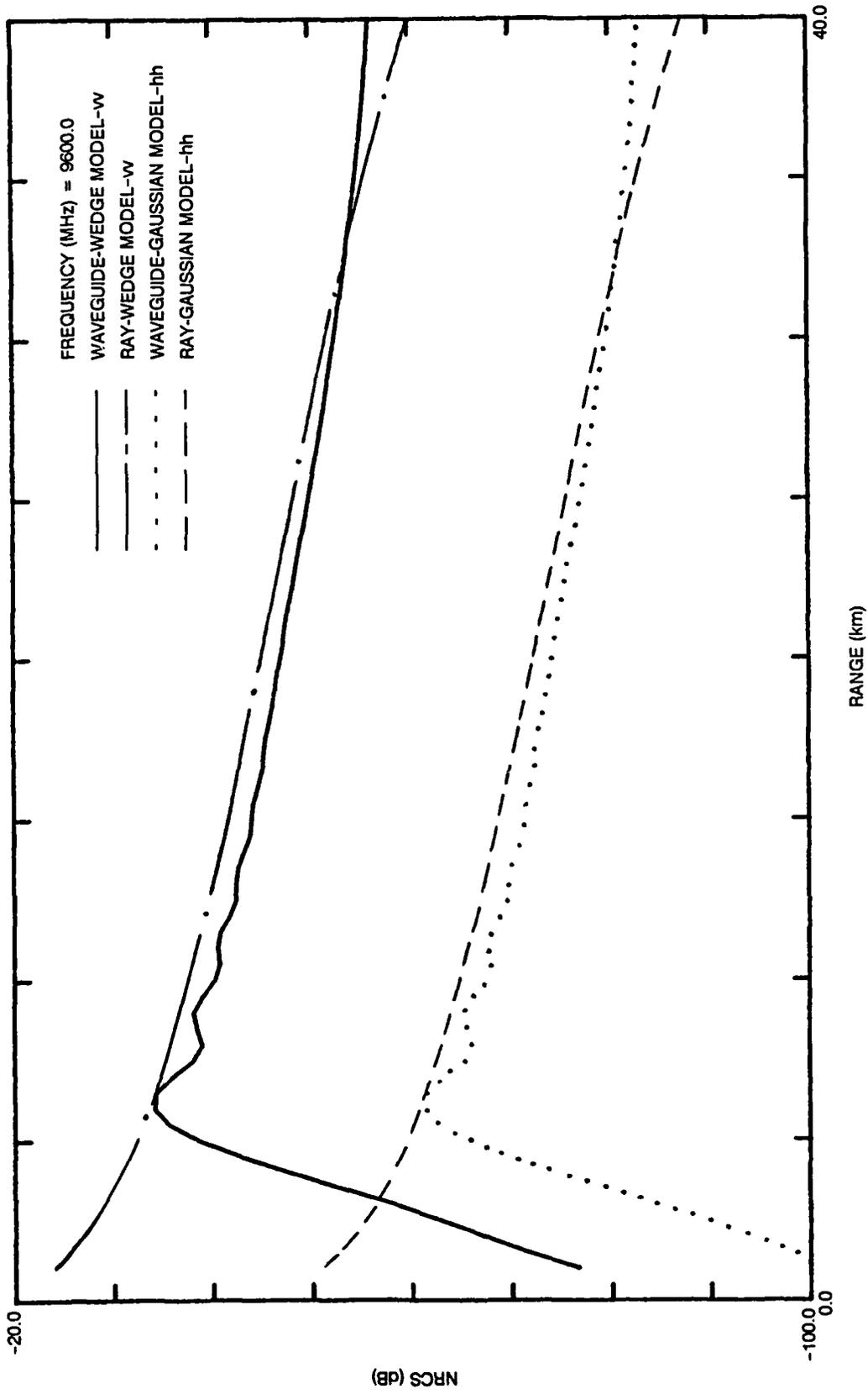
28

Figure 18. Normalized radar cross section versus range. Ray and waveguide model comparisons. Fourteen meter duct with 20-knot wind.
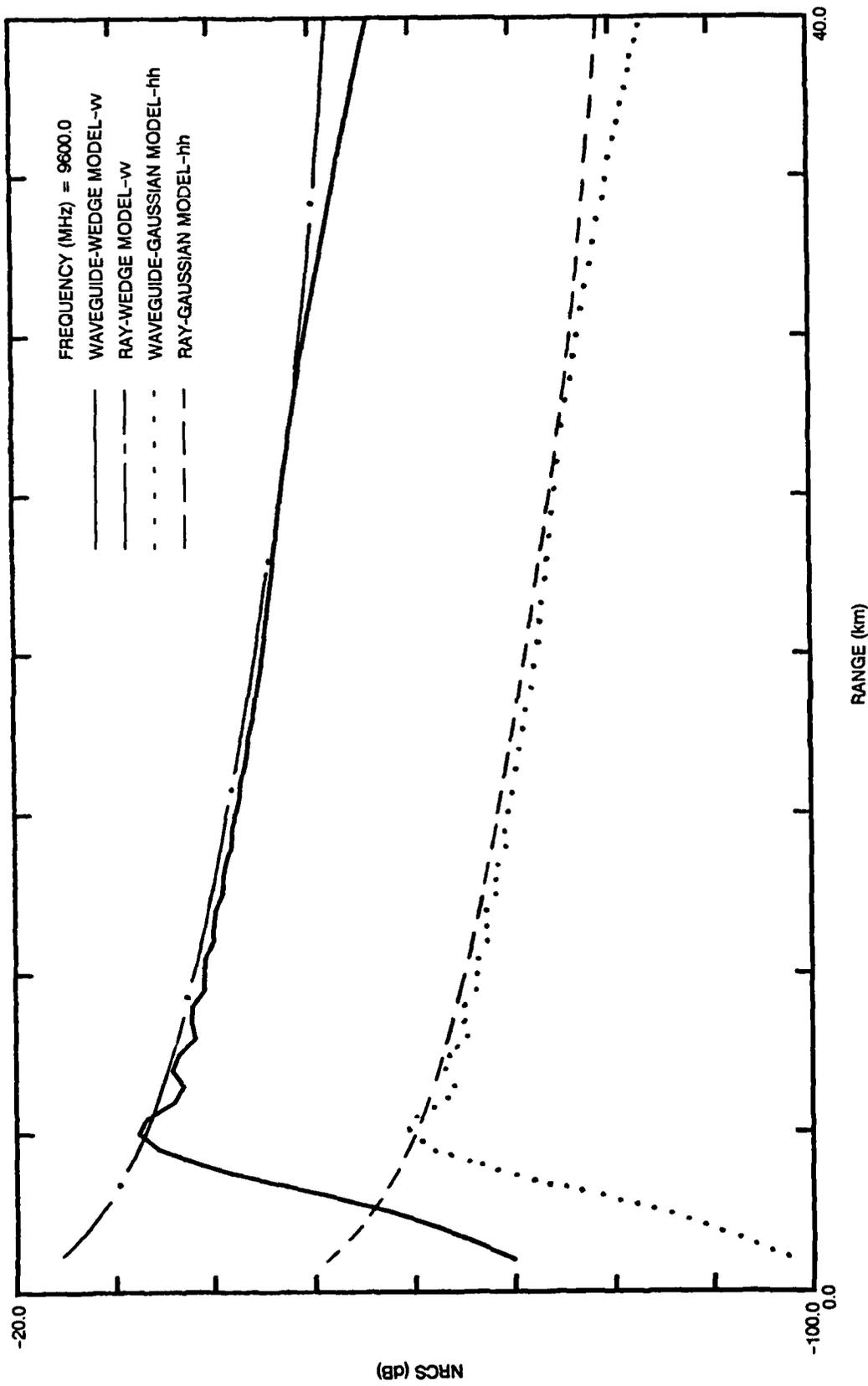
29

Figure 19. Normalized radar cross section versus range. Ray and waveguide model comparisons. Twenty-eight-meter duct with 20-knot wind.
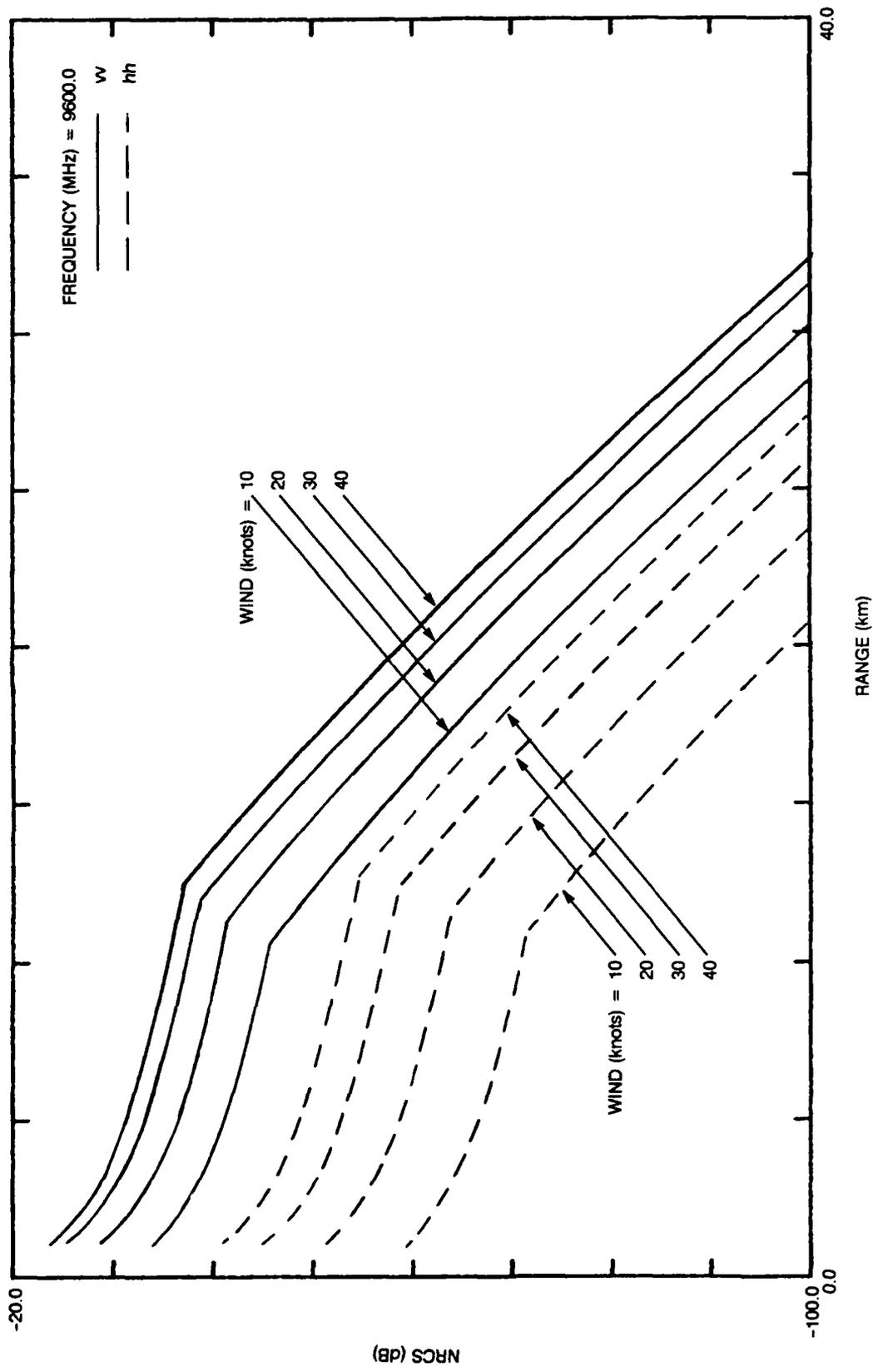
Figure 20. Normalized radar cross section versus range. Ray/Waveguide-Gaussian model results with wind speed as a parameter. Standard atmosphere.
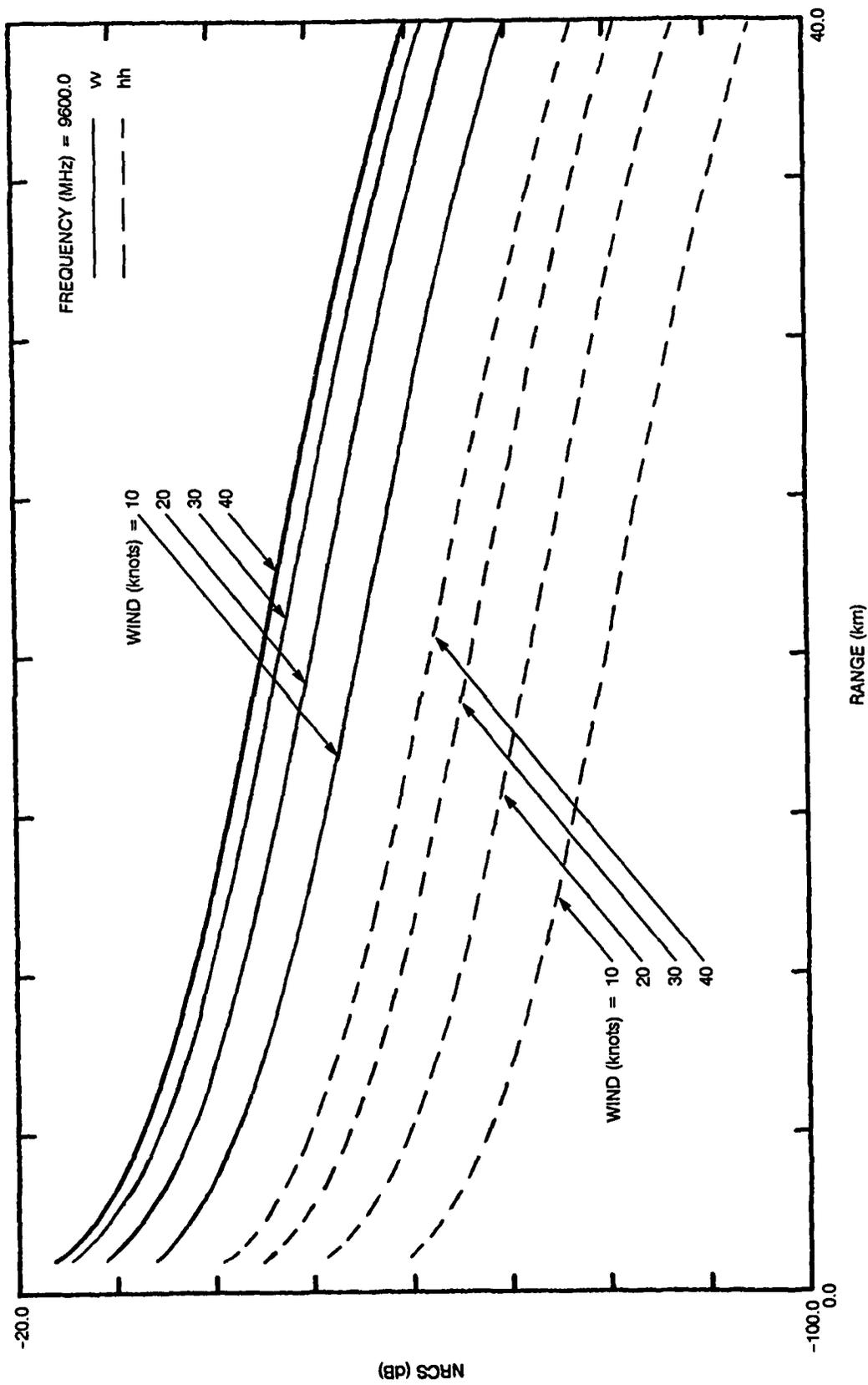
31

Figure 21. Normalized radar cross section versus range. Ray-Gaussian model results with wind speed as a parameter. Fourteen-meter duct.
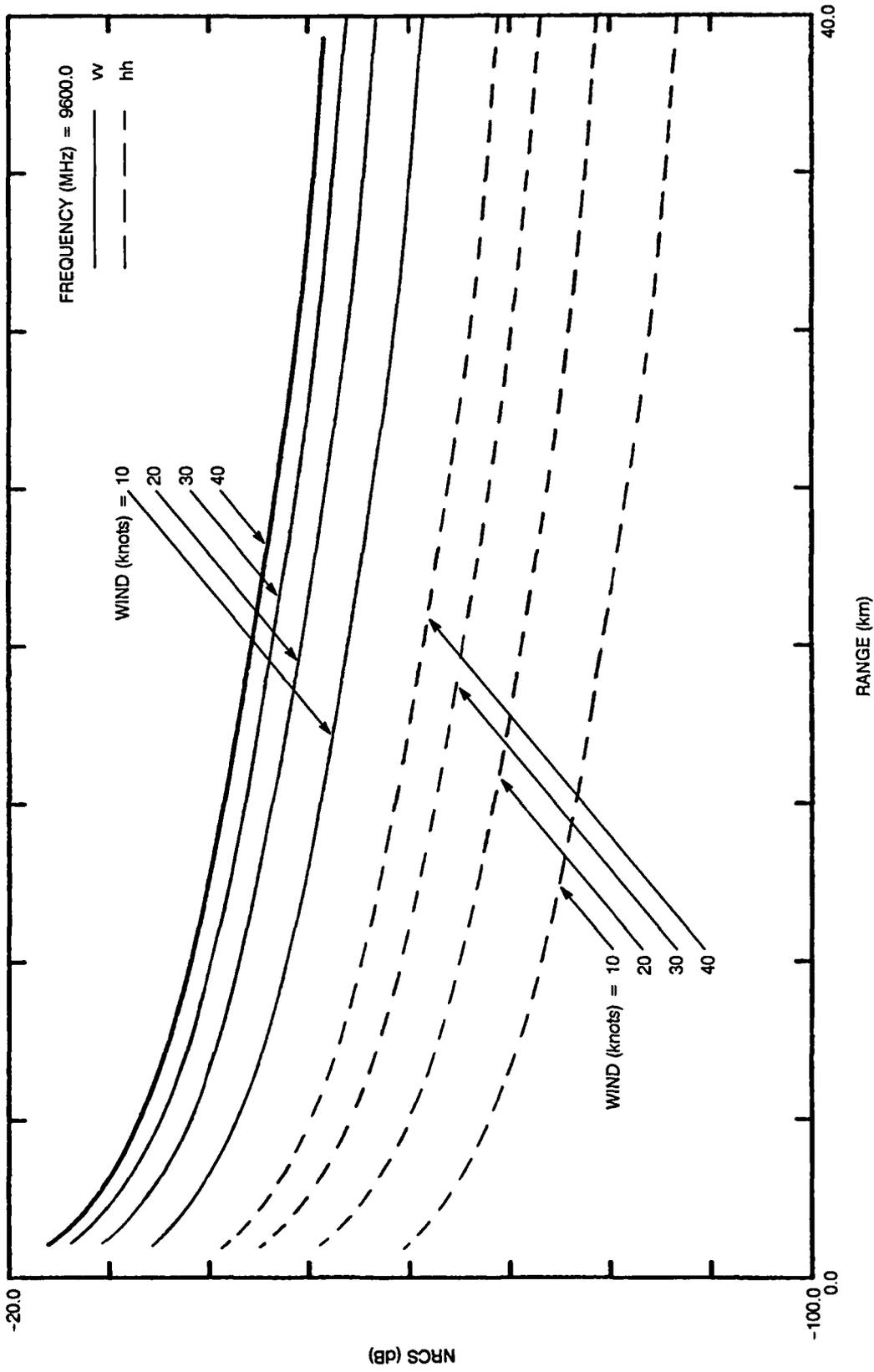
32

Figure 22. Normalized radar cross section versus range. Ray-Gaussian model results with wind speed as a parameter. Twenty-eight-meter duct.
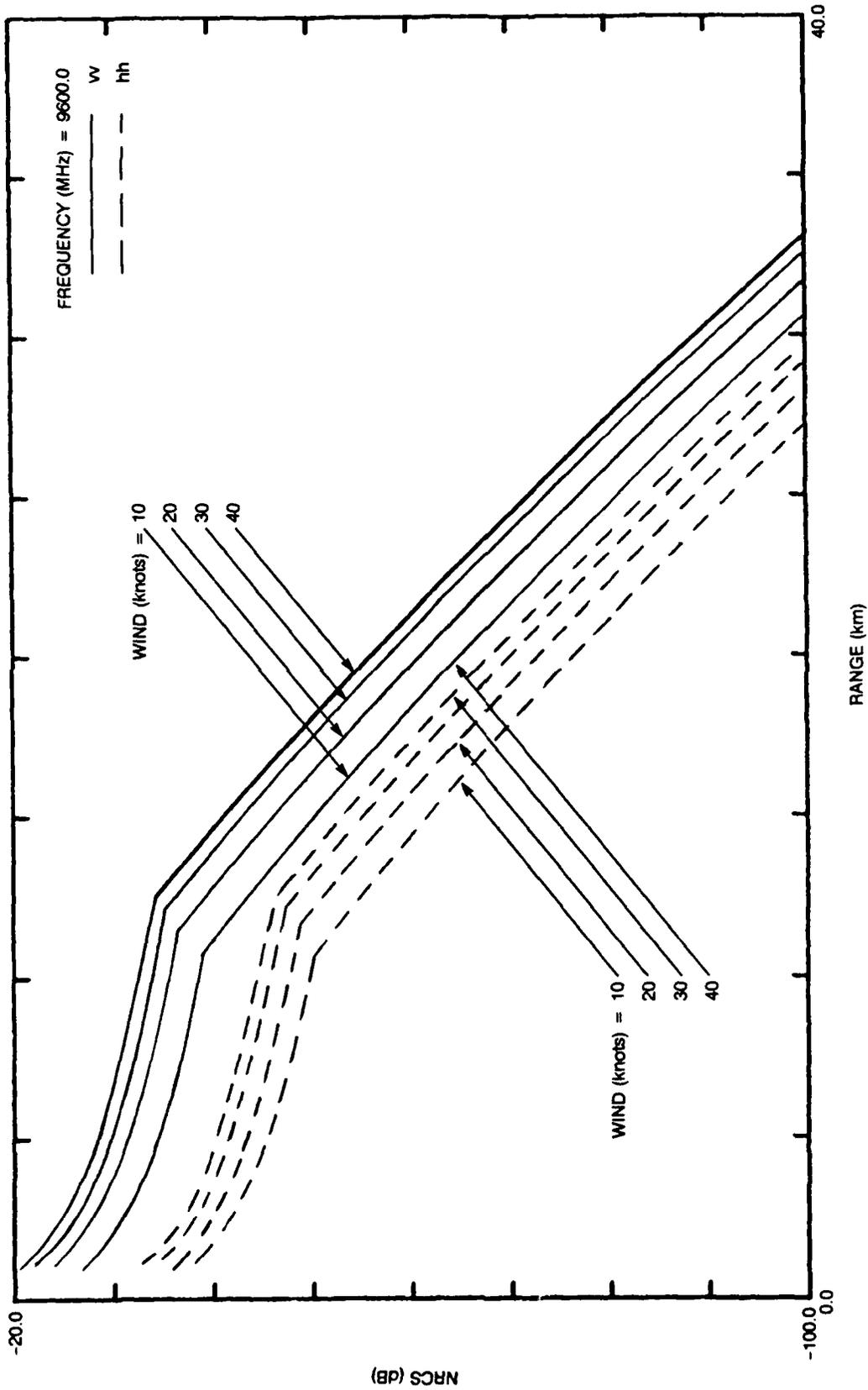
33

Figure 23. Normalized radar cross section versus range. Ray/Waveguide-wedge model results with wind speed as a parameter. Standard atmosphere.
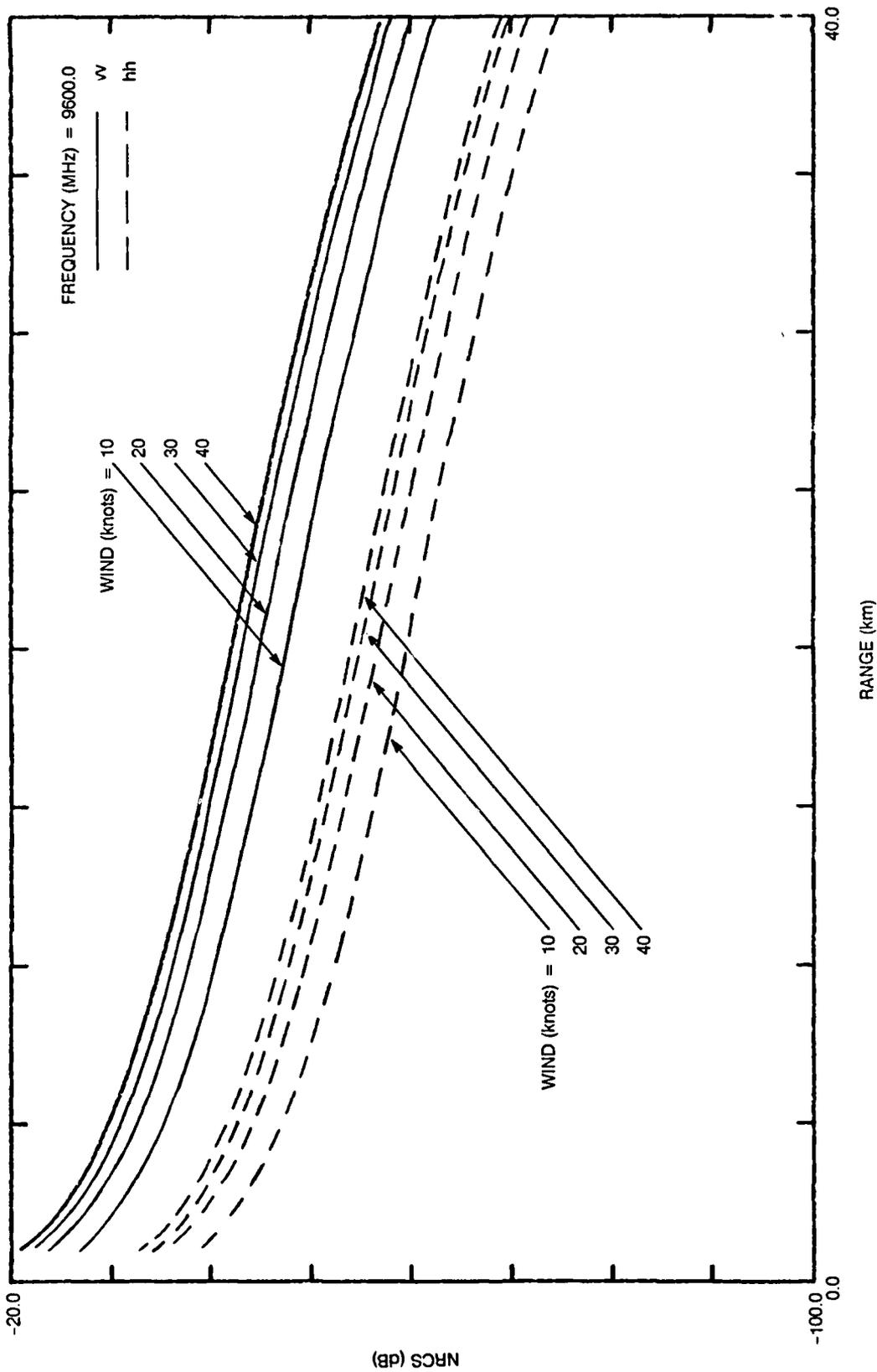
Figure 24. Normalized radar cross section versus range. Ray-wedge model results with wind speed as a parameter. Fourteen-meter duct.
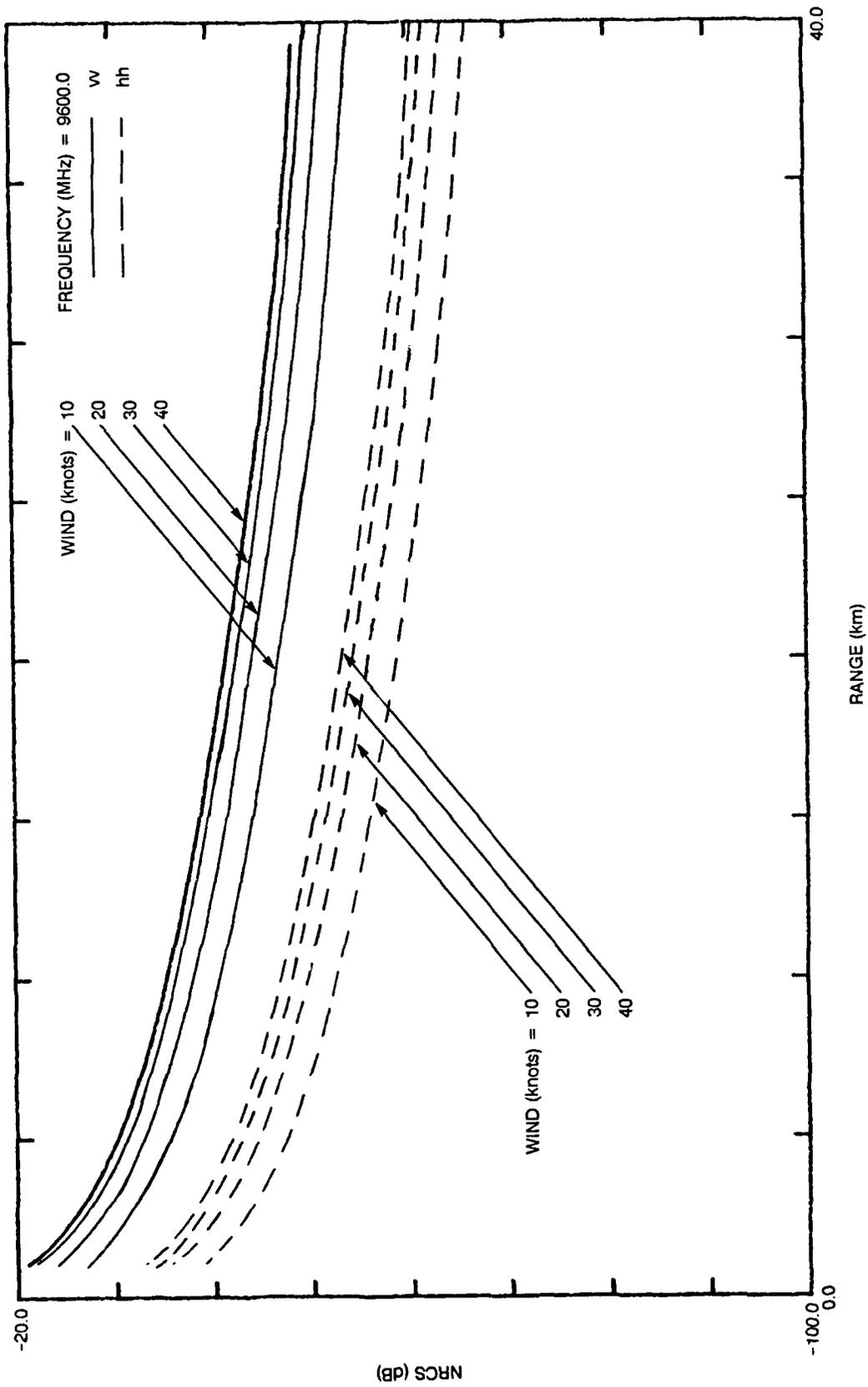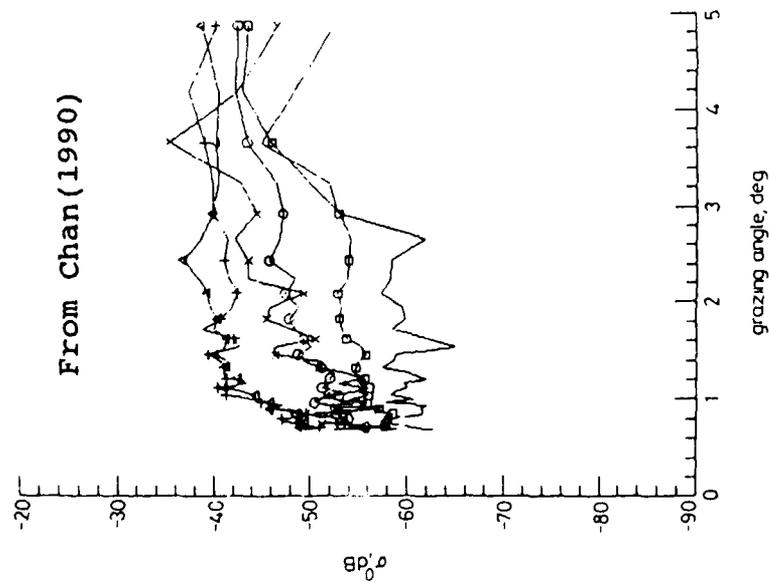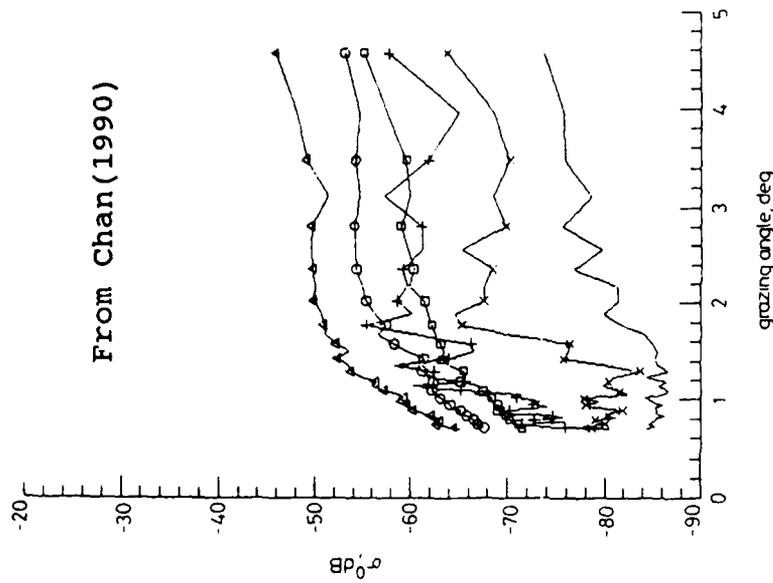
Figure 25. Normalized radar cross section versus range. Ray-wedge model results with wind speed as a parameter. Twenty-eight-meter duct.

36

From Chan(1990)

Date = 12th July 1982; time = 16:04:58 (V-Pol), 16:10:23 (H-Pol)

		Azimuth	AVG Doppler
—△—		120°	15 Hz
—○—	V-Pol	75°	5 Hz
—□—		30°	-5 Hz
—+—		120°	40 Hz
—×—	H-Pol	75°	25 Hz
———		30°	-10 Hz

Figure 27. Typical $\sigma°$ against grazing angle profiles of s-band sea-clutter in the upswell and near-cross-swell directions.

From Chan(1990)

Date = 12th July 1982; time = 16:24:15 (V-Pol), 16:30:17 (H-Pol)

		Azimuth	Average Doppler
—△—		120°	50 Hz
—○—	V-Pol	75°	30 Hz
—□—		30°	-5 Hz
—+—		120°	90 Hz
—×—	H-Pol	75°	70 Hz
———		30°	0 Hz

Figure 26. Typical $\sigma°$ against grazing angle profiles of x-band sea-clutter in the upswell and near-cross-swell directions.

37

REPORT DOCUMENTATION PAGE

Public reporting burden for this collection of information is estimated to average 1 hour per response, including the time for reviewing instructions, searching existing data sources, gathering and maintaining the data needed, and completing and reviewing the collection of information. Send comments regarding this burden estimate or any other aspect of this collection of information, including suggestions for reducing this burden, to Washington Headquarters Services, Directorate for Information Operation, and Reports, 1215 Jefferson Davis Highway, Suite 1204, Arlington, VA 22202-4302, and to the Office of Management and Budget, Paperwork Reduction Project (0704-0188), Washington, DC 20503.

1. AGENCY USE ONLY (Leave blank)	2. REPORT DATE	3. REPORT TYPE AND DATES COVERED
	January 1991	Final

4. TITLE AND SUBTITLE

SEA ECHO CALCULATIONS FOR HH AND VV POLARIZATION

5. FUNDING NUMBERS

PE: 0602435N
WU: DN488 760

6. AUTHOR(S)

R. A. Pappert

7. PERFORMING ORGANIZATION NAME(S) AND ADDRESS(ES)

Naval Ocean Systems Center
San Diego, CA 92152-5000

8. PERFORMING ORGANIZATION REPORT NUMBER

NOSC TD 2034

9. SPONSORING/MONITORING AGENCY NAME(S) AND ADDRESS(ES)

Office of Naval Technology
Arlington, VA 22217

10. SPONSORING/MONITORING AGENCY REPORT NUMBER

11. SUPPLEMENTARY NOTES

12a. DISTRIBUTION/AVAILABILITY STATEMENT

Approved for public release; distribution is unlimited.

12b. DISTRIBUTION CODE

13. ABSTRACT (Maximum 200 words)

Surface normal tilting perpendicular to the unperturbed plane of incidence has the effect that an incident horizontally (vertically) polarized wave presents both polarization types to the local scattering facet. Thus, for such a surface, backscatter, even for a horizontally or vertically polarized incident wave, results from incidence of both polarizations on the locally perturbed surface. Impact of this effect on HH and VV backscatter is examined within the context of composite model formalism and previously developed ray and waveguide path loss formulas. Results are given for an x-band frequency for standard and evaporation duct environments at windspeeds of 10, 20, 30, and 40 knots.

14. SUBJECT TERMS

plane of incidence
polarization incident work

15. NUMBER OF PAGES

42

16. PRICE CODE

17. SECURITY CLASSIFICATION OF REPORT	18. SECURITY CLASSIFICATION OF THIS PAGE	19. SECURITY CLASSIFICATION OF ABSTRACT	20. LIMITATION OF ABSTRACT
UNCLASSIFIED	UNCLASSIFIED	UNCLASSIFIED	SAME AS REPORT

INITIAL DISTRIBUTION

Code 0012   Patent Counsel   (1)
Code 0144   R. November   (1)
Code 54   J. Richter   (5)
Code 541   F. Ryan   (1)
Code 542   R. Pappert   (2)
Code 542   J. Ferguson   (1)
Code 542   C. Shellman   (1)
Code 543   H. Hitney   (1)
Code 543   K. Anderson   (1)
Code 543   R. Paulus   (1)
Code 543   C. Hattan   (1)
Code 543   W. Patterson   (1)
Code 961   Archive/Stock   (6)
Code 964   Library   (3)

Defense Technical Information Center   (4)
Alexandria, VA   22304-6145

NOSC Liaison Office
Washington, DC   20363-5100   (1)

Center for Naval Analyses
4401 Ford Avenue
Alexandria, VA   22302-0268   (1)